research articles Journal of proteome research

Combined NMR and LC-MS Analysis Reveals the Metabonomic Changes in *Salvia miltiorrhiza* Bunge Induced by Water Depletion

Hui Dai,[†,§] Chaoni Xiao,[†,‡,§] Hongbing Liu,[†,§] and Huiru Tang*[,†]

State Key Laboratory of Magnetic Resonance and Atomic and Molecular Physics, Wuhan Centre for Magnetic Resonance, Wuhan Institute of Physics and Mathematics, Chinese Academy of Sciences, Wuhan 430071, P.R.China, College of Life Sciences, Northwest University, Xi'an 710069, P.R. China, and Graduate University of the Chinese Academy of Sciences, Beijing 100049, P.R. China

Received November 3, 2009

Plant metabonomic analysis is essential for understanding plant systems responses to osmotic stresses. To understand the comprehensive metabolic responses of *Salvia miltiorrhiza* Bunge (SMB) to continuous and exhaustive water depletion, we characterized the SMB metabonomic variations induced by three different drying processes using the combined NMR and LC-DAD-MS method. NMR results showed that SMB extracts were dominated by 29 primary metabolites such as sugars, carboxylic acids and amino acids, which were comprehensively reported for the first time, and 8 secondary metabolites including polyphenolic acids and diterpenoids. LC-DAD-MS methods detected 44 secondary metabolites, among which 5 polyphenolic acids together with genipin, umbelliferone and tormentic acid were found for the first time in this plant. We found that aqueous methanol was efficient in extracting both primary metabolites and polyphenolic acids, whereas chloroform−methanol was effective in selectively extracting diterpenoids. We further found that air- and sun-drying markedly affected both primary and secondary metabolisms of SMB by enhancing tanshinone and glutamate-mediated proline biosynthesis and altering carbohydrate and amino acid metabolisms. The shikimate-mediated biosynthesis of polyphenolic acids was promoted by air-drying but suppressed by sun-drying. These findings fill the gap of our understandings to the metabolic responses of *S. miltiorrhiza* Bunge to water depletion and demonstrated effectiveness of the combined NMR and LC-DAD-MS methods in plant metabonomic analysis.

Keywords: *Salvia miltiorrhiza* Bunge • NMR • LC-DAD-MS • PCA (principal component analysis) • OPLS-DA (orthogonal projection to latent structure with discriminant analysis)

Introduction

Water depletion is a typical osmotic stress to plant cells causing profound systemic responses. The published transcriptomic and proteomic results indicate that such stressors often affect plant cell development and self-protections by altering many physiological processes related to the cell wall modifications,[1] signal transductions[2] and protein folding.[3] Functional analysis for these changes also strongly implied the metabolic responses to such stressors.[4,5] Plant metabonomics approaches ought to have important roles to play in such analysis since metabonomics is a branch of science concerning the total metabolite pool (metabonome) of integrated biological systems and dynamic responses to the alterations of endogenous and/or exogenous factors.[6,7] In fact, metabonomics has already been established as a powerful tool for understanding the toxin- and stress-induced mammalian metabonomic changes,[8,9] gene functions,[10,11] mammalian pathophysiology[12−14] and in environmental science.[15,16] Applications have also been successfully realized in the composition-based quality controls and authentication of food products[17−19] and phytomedicines.[20−23]

Plant metabonomic analyses still face many challenges, although progress has been made during past years. These challenges arise from the complexity of the plant metabolite composition (metabonome) and limitations of a given analytical method. On one hand, the metabonome of plants often consists of both primary and secondary metabolites; the holistic plant metabonomic analysis requires complete determination of both classes of metabolites. On the other hand, neither of two existing main stream methods (i.e., NMR and LC-DAD-MS) alone can fully meet such requirements due to their intrinsic limitations in either detection or quantification. NMR techniques are generally rapid with rich structure information and capable of measuring all the abundant metabolites in a single spectrum. Its intrinsically low sensitivity, however, makes it unfavorable for detecting metabolites at the submicromolar (sub-μM) level unless some sample pretreatments are employed. In contrast, the LC-DAD-MS methods are metabolite selective owing to variable response coefficients and biased for

* To whom correspondence should be addressed. E-mail: huiru.tang@wipm.ac.cn. Telephone: +86-(0)27-87198430. Fax: +86-(0)27-87199291.
† Wuhan Institute of Physics and Mathematics, Chinese Academy of Sciences.
§ Graduate University of the Chinese Academy of Sciences.
‡ Northwest University.

10.1021/pr900995m

Published on Web 01/03/2010

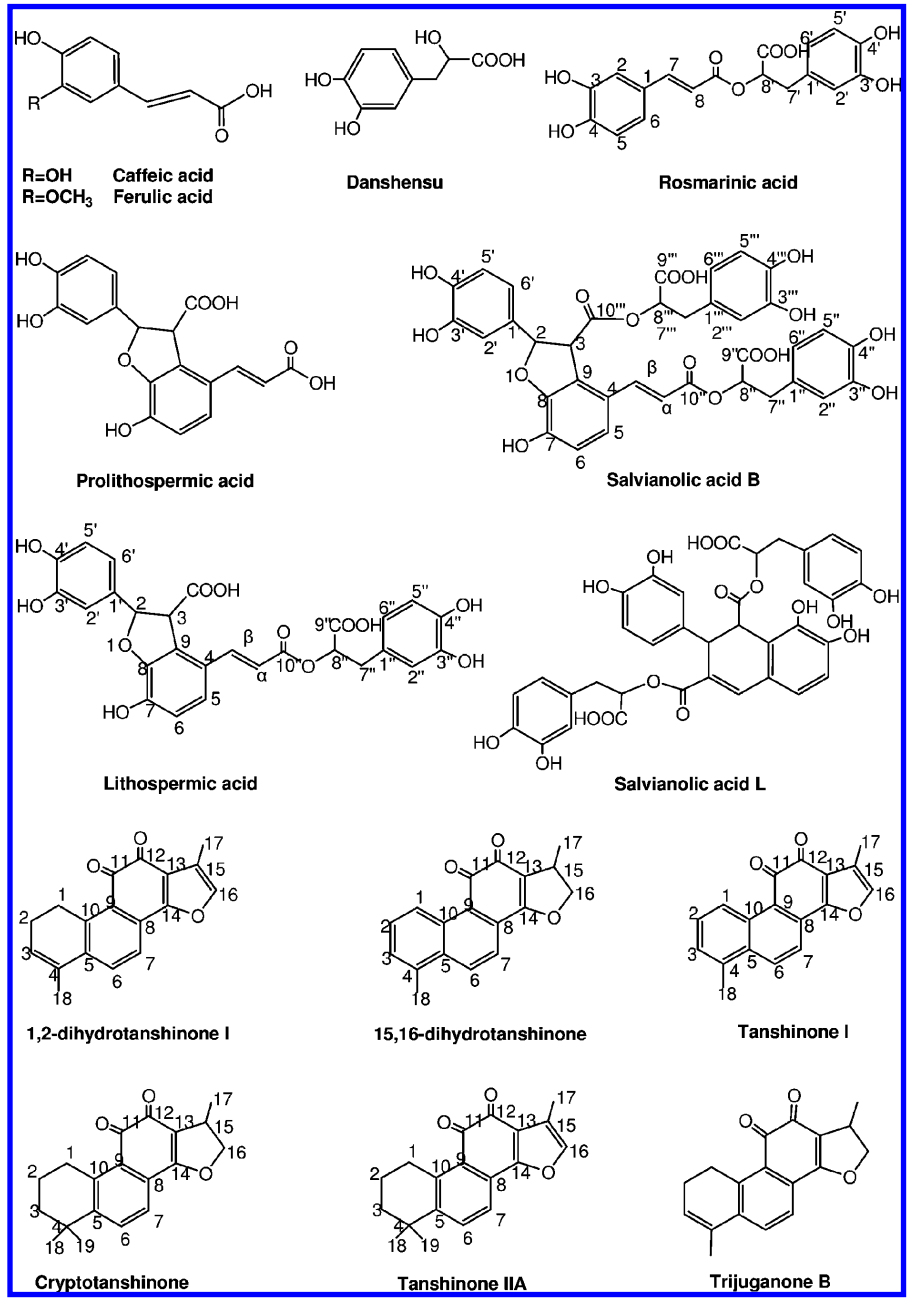

Figure 1. The structures of some secondary metabolites of *SMB*.

those with high response coefficients; standards and *in situ* calibration curves (for each metabolite) are often required in identification and quantification of different metabolites. In practice, however, not all such standards are available. Nevertheless, such selectivity can be advantageous in targeted analyses for detecting the low-concentration metabolites which cannot be detected otherwise. It is thus conceivable that the combination of NMR and LC-DAD-MS may offer some complementary advantages in plant metabonomic analysis, although few studies have yet been reported to explore the advantages of such combination.

The medicinal plant *Salvia miltiorrhiza* Bunge (SMB) is an excellent challenging example for efficient plant metabonomic analysis due to its complex metabonome consisting of many primary and secondary metabolites. The dry roots of SMB were widely used as phytomedicine for the treatments of atherosclerosis,[24] myocardial ischemia[25] and hepatic fibrosis[26] owing to the free-radical scavenging properties[27] of its secondary metabolites including dozens of polyphenolic acids such as salvianolic acids and diterpenoids in the forms of tashinones,[28] the structures of which (Figure 1) were well-characterized in the classical phytochemistry studies.[29,30] However, all these studies have focused exclusively on the SMB's secondary metabolites without considering its primary metabolites, although plant primary metabolism has profound effects on the secondary one[31,32] and carries important information on plant physiology. Many primary metabolites such as amino acids and organic acids (e.g., TCA cycle intermediates) are also human endogenous metabolites and their intakes during medicinal treatments will have collective effects on human biochemistry.

Furthermore, phytomedicines are often air- or sun-dried for the purposes of transportation, storage and pharmacological requirements. Such drying processes will conceivably result in adaptation responses of plant cells to drying-induced osmotic

stress, thus, plant metabonomic alterations. Such notion has been well reflected by the drying induced decreases in the total phenolic contents in *Phyllanthus amarus*,[33] *Eugenia uniflora*[34] and dietary herbs,[35] though no details were offered there on specific responsive compounds. Previous work also showed that drying processes caused marked rosemary metabonomic changes in both its primary and secondary metabolism.[31] However, the effects of water depletion on the metabolite composition of *S. miltiorrhiza* Bunge remain to be fully elucidated.

Moreover, solvent extraction is often a prerequisite for plant metabonomic studies and the different extraction methods and solvents may have marked impacts on extraction efficiency for different metabolites. Previous studies have already shown the extractability dependence on extraction methods[36,37] for SMB metabolites. For example, the microwave-assisted extraction (MAE) favored tanshinones yield[37] and polar solvents (water and ethanol) favored extracting polyphenolic acids, whereas nonpolar solvents (ethyl acetate and hexane) were preferred for tanshinones. However, all these studies were focused on a few selected secondary metabolites and little has been reported on the systematic evaluations of the solvent effects on the metabolite composition of SMB extracts especially when both primary and secondary metabolites are concerned. As SMB is normally administered as decoction (i.e., hot water extracts) and alcoholic maceration (i.e., aqueous ethanol extracts), classic studies of SMB secondary metabolites extracted with methanol, chloroform and hexane may not be relevant.

In this study, we have systematically characterized variations of SMB metabonome with extraction solvents and drying processes using the combination of NMR and LC-DAD-MS methods in conjunction with multivariate data analysis. The aims are to (1) explore the feasibility of the combined NMR and LC-DAD-MS methods for plant metabonomic analysis, (2) obtain all the detectable SMB metabolites with the combined advantages of both techniques, and (3) define the effects of different drying processes and extraction solvents on the SMB metabonome.

Materials and Methods

Chemicals. Methanol, ethanol, chloroform, formic acid, $K_2HPO_4 \cdot 2H_2O$ and $NaH_2PO_4 \cdot 12H_2O$ (all analytical grade) were purchased from Guoyao Chemical Co. Ltd. (Shanghai, China). HPLC-grade acetonitrile was bought from J. T. Baker Pharmaceuticals Company (Phillipsburg, NJ) and the water used for HPLC was obtained from a Milli-Q system (Millipore, Milford, MA). Deuterated chloroform ($CDCl_3$, 99.9% D) containing tetramethylsilane (TMS, 0.03%, m/v), D_2O (99.9% D) and sodium 3-trimethlysilyl [2,2,3,3-d_4] propionate (TSP) were purchased from Cambridge Isotope Laboratories, Inc. (Andover, MA).

Materials and Sample Preparation. To investigate the solvent effects on metabolite compositions of the resultant SMB extracts, the dried roots of *S. miltiorrhiza* Bunge (SMB) from a local pharmacy were employed. To investigate the effects of drying processes on the metabolite compositions, the fresh roots of SMB were purchased from a nationally certified cultivation base (Zhongjiang, Sichuan, China). These fresh samples were subjected to freeze-drying after snap-frozen in liquid nitrogen, sun-drying and air-drying under good ventilation (sample information is tabulated in Supporting Information Table S1). The drying period was normally about 2−3 days. The dried materials were then sealed in plastic bags, separately, and stored in dry and dark conditions until analysis.

All the dried SMB materials were ground with a coffee blender and then sieved through a 2 mm sieve. To investigate the effects of extraction solvents on the SMB metabonome, the same dried raw materials were divided into five portions, and each portion (about 1 g) was extracted ultrasonically (i.e., 1 min sonication with 1 min break) for 30 min with 15 mL of boiling water (solvent A), 50% aqueous ethanol (solvent B), 50% aqueous methanol (solvent C) and chloroform−methanol mixture (3:1, v/v) (solvent D), respectively. The resultant extracts were denoted as A, B, C, and D, respectively (see Supporting Information Table S1 for sample information). For the boiling water extraction, the water temperature was allowed to decrease naturally during the process without interference. The freeze-dried, air-dried, and sun-dried SMB materials were extracted with solvent C to evaluate the effects of drying processes on the SMB metabonome. The supernatants were collected after 10 min centrifugation (10000 rpm with a benchtop centrifuge) and the solid residues were further extracted twice using the same procedure. After combining the three obtained solution, the extracts from solvent A were lyophilized directly, whereas the organic solvents in the samples from solvents B, C, and D were removed individually at 30 °C with a rotary evaporator before lyophilization. Five extracts were obtained for each of the groups.

NMR Measurements. The SMB extracts (∼2 mg) from solvents A, B, and C were dissolved in 600 μL of phosphate buffer (0.1 M, pH 7.4, K_2HPO_4-NaH_2PO_4) containing 10% D_2O and TSP (0.2 mM), whereas the chloroform−methanol extracts (∼10 mg) were dissolved in 600 μL of $CDCl_3$ containing 0.03% TMS. The samples were then centrifuged for 10 min before the supernatants (550 μL) were transferred into 5 mm NMR tubes for NMR analysis. ^{1}H NMR spectra were acquired at 298 K on a Bruker AV III 600 MHz NMR spectrometer equipped with a cryogenic inverse probe. A standard one-dimensional pulse sequence (RD-90°-t_1-90°-t_m-90°-acquisition) was employed with a weak irradiation on the water peak during the recycle delay (RD, 2 s) and the mixing time (t_m, 100 ms) to suppress water signal. The parameter t_1 was set to 4 μs and 90° pulse length was adjusted to about 10 μs for each sample. A total of 64 transients were acquired into 32k data points with a spectral width of 11999.4 Hz and an acquisition time of 1.36 s. An exponential window function with line broadening factor of 0.3 Hz was applied to the free induction decays (FID) prior to Fourier transformation (FT).

For spectral resonance assignment purposes, ^{1}H−^{1}H correlation spectroscopy (COSY), ^{1}H−^{1}H total correlation spectroscopy (TOCSY), ^{1}H *J*-resolved, ^{1}H−^{13}C HSQC and HMBC 2D NMR spectra were acquired on selected samples. In COSY and TOCSY experiments, 48 transients for each of 128 increments were collected into 2048 (2k) data points with spectral width of 6313 Hz. MLEV-17 was employed as spin-lock scheme in TOCSY experiment with the mixing time of 80 ms. For *J*-resolved spectra, 32 transients for each of 50 increments were collected into 2k data points with spectral width of 6313 Hz in F_2 (chemical shift dimension) and 50 Hz in F_1 (J coupling constant dimension). ^{1}H−^{13}C HSQC and HMBC 2D NMR spectra were recorded using the gradient selected pulse sequences. In HSQC experiments, composite pulse broadband ^{13}C decoupling (globally alternating optimized rectangular pulses, GARP) was employed during the acquisition period; 240 transients for each of 128 increments were collected into 2k

data points with spectral width of 6313 Hz in ^{1}H dimension and 26410 Hz in the ^{13}C dimension. In HMBC experiments, a total of 400 transients were collected into 2k data points for each of 128 increments with spectral width of 6313 Hz in ^{1}H dimension and 33201 Hz in the ^{13}C dimension with the long-range coupling constant of 6 Hz. These data were zero-filled to 2k data points in the evolution dimension prior to appropriate apodization and FT with forward linear prediction.

Spin−lattice relaxation times (T_1) of metabolites in the extracts were measured using the classical "inversion recovery" sequence (RD-180°-τ-90°-acquisition) with water suppressed during both recycle delay (RD) and relaxation delay τ. Sixteen τ values of 0.1−14.5 s were employed with the total repeat time of 21.4 s (including both recycle delay and acquisition time) and 32 scans were acquired for each sample over 32k points. The areas from the top of peaks (about 8 points) were used to calculate the T_1 values by fitting experimental data into a single exponential relaxation process (for the least overlapping resonances).

Quantification of Metabolites. It is well-known that the integral of a given ^{1}H NMR signal is directly and linearly proportional to the number of protons which give such signal. Therefore, the concentration of metabolites can be measured by equating the peak areas of them and a reference compound with known concentration. The metabolite concentration can also be measured in an incompletely relaxed ^{1}H NMR spectrum with known relaxation times for both analytes and reference. With the effective magnetization reading pulse of 90° in this study, the integral area for a given proton resonance in an incompletely relaxed NMR spectra obeys the following equation (eq 1):

$$A^m = A_0^m[1 - \exp(-t/T_1^m)] \quad (1)$$

where t is total relaxation time (i.e., recycle delay plus acquisition time); A^m and A_0^m are signal integral areas in a given spectrum and the completely relaxed one, respectively, for proton m with a spin−lattice relaxation time of T_1^m. With the known concentration of an internal reference (i.e., TSP in our case), the integral areas for a given proton signal and TSP will have following relationship (eq 2):

$$\frac{A_0^m}{A_0^{TSP}} = \frac{A^m}{A^{TSP}} \frac{1 - \exp(-t/T_1^{TSP})}{1 - \exp(-t/T_1^m)} \quad (2)$$

where A_0^{TSP} and A^{TSP} are the integral area for methyl groups of TSP in the completely and incompletely relaxed spectra, respectively; T_1^{TSP} is the spin−lattice relaxation time for methyl protons of TSP. The concentration of a metabolite and TSP in the same spectra follows the relationship described in eq 3 taking into consideration of the proton numbers related to relevant NMR signals (eq 3),

$$C_m = \frac{N_{TSP} C_{TSP} A_0^m}{N_m A_0^{TSP}} \quad (3)$$

where C_m and C_{TSP} are concentration of a given metabolite and TSP, respectively; N_m and N_{TSP} denote proton numbers from the protons of metabolite and from methyl groups of TSP (i.e., 9 protons), respectively. By combining the eqs 1−3, the concentration of a given metabolite can be readily calculated from the signal areas and the T_1 values for the metabolites and TSP. The errors for metabolite quantity measured with the NMR methods here were estimated to be well below 15% using salvianolic acid B solutions (0.3597 and 1.4406 mM).

LC-DAD-MS Measurements. The LC-DAD-MS measurements were performed on an Agilent 1200 system (Agilent Technologies, Waldbronn, Germany) coupled with a Bruker microQTOF mass spectrometer (Bruker Daltonics, Germany) with an ESI interface. The LC system consists of a quaternary solvent delivery system, an online degasser, an autosampler, a column temperature controller and a diode-array detector (DAD). An ACE C18-HL column (5 μm, 250 × 4.6 mm) was used with a C18 guard column, column temperature of 30 °C and the sample injection volume of 10 μL (about 5 mg/mL). The monitoring wavelength was 280 nm with the acquisition wavelength for the DAD set to about 210−600 nm. The mobile phases consisted of water (A) and acetonitrile (B) both containing 0.1% (v/v) formic acid. A stepped solvent gradient was used as follows: 0−0.5 min, 5% B; 0.5−40 min, 5−37% B; 40−50 min, 37−60% B; 50−55 min, 60−74% B; 55−68 min, 74−80% B; 68−75 min, 80−83% B. The flow rate was 1.0 mL/min with 5% of the eluant directed to MS using a BNMI unit (Bruker BioSpin, Germany). The optimized mass spectrometric parameters were as follows: nebulizer gas pressure 0.8 bar, drying gas flow rate 8 L/min, gas temperature 180 °C and capillary voltage 4500 V in the negative ion mode whereas −4000 V in the positive ion mode. The spectral range was set to m/z 50−1000.

Multivariate Data Analysis. Following Fourier Transformation and referencing to TSP or TMS (δ0.0), the ^{1}H NMR spectra were corrected for phase and baseline distortions manually using Topspin (v2.0, Bruker Biospin, Germany). The spectra (0.5−10 ppm) were then divided into integral regions with equal width of 0.004 ppm (2.4 Hz) using the AMIX package (v.3.8.3, Bruker Biospin). For SMB extracts from hydrophilic solvents, the spectral regions δ4.20−5.236 and δ5.28−5.4 were excluded to remove the effects of imperfect water suppression. The residual solvent signals from CH_3OH (δ3.344−3.388), C_2H_5OH (δ3.632−3.70, δ1.06−1.312) and $CHCl_3$ (δ7.20−7.33) were also discarded. For SMB extracts from different drying processes, the regions δ4.704−4.968 and δ3.344−3.388 were removed to eliminate the residual water and CH_3OH signals, respectively.

The NMR data were normalized to the total sum of the spectral integrals prior to data analyses to compensate for the concentration differences. Multivariate data analysis was carried out using the SIMCA-P$^+$ software package (v.11, Umetrics; Umea, Sweden). Principal component analysis (PCA) was conducted for the normalized data using mean-centered data. Data were visualized by means of principal component (PC) scores plots, where each point represented an individual sample (or its metabonome), and loadings plots where differential metabolite peaks were shown as positive and negative signals to indicate the relative changes of metabolites. Orthogonal projection to latent structure with discriminant analysis[38] (OPLS-DA) was further conducted using the NMR data (scaled to unit variance) as X-matrix and the class information as dummy Y-variables. The quality of the model was described by the 5-fold cross-validation parameter Q^2, indicating the predictability of the model, and R^2X representing the total explained variables for the X-matrix. The loadings were calculated by back-transformation as described previously.[39] The coefficient-coded loadings plot were constructed with an MATLAB script downloaded from http://www.mathworks.com/

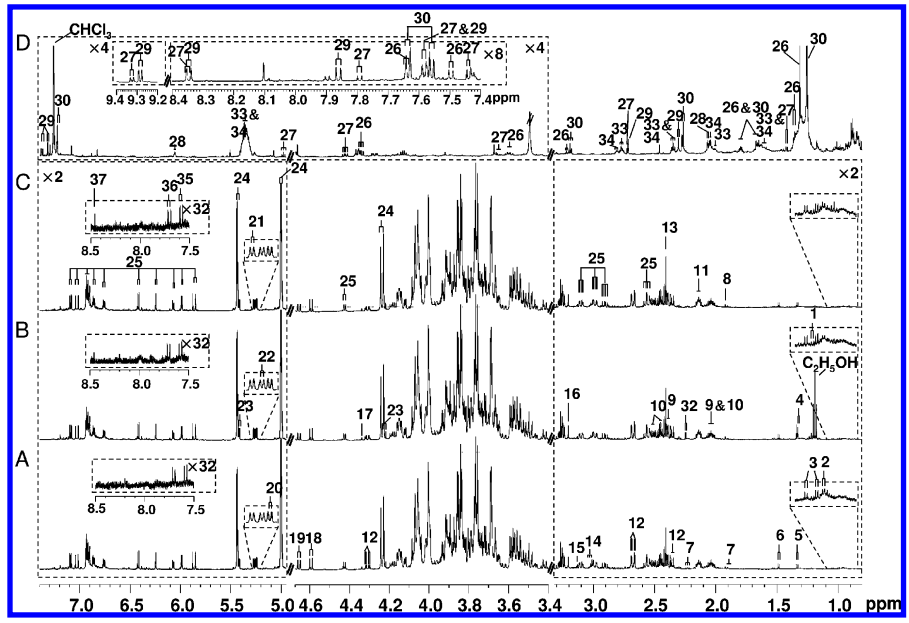

Figure 2. 600 MHz ^{1}H NMR spectra of SMB extracts from boiling water (A), 50% aqueous ethanol (B), 50% aqueous methanol (C) and chloroform−methanol (v/v, 3/1) (D). For A, B, and C, the spectral regions δ3.22−0.88 and δ7.40−4.95 were expanded for 2 times, while δ8.50−7.50 region was expanded 32 times; for D, the regions δ7.40−3.40 and δ9.40−9.20 were expanded 4 times and δ8.40−7.40 was expanded 8 times (see Table 1 for metabolite identification key).

with some in-house modifications and color-coded with square value of coefficients (r^2), where the coefficients describe the weighting of variables contributing the discrimination in the models. This allows each variable to be plotted with color-coding to show the significance of class discrimination as calculated from the correlation matrix. In this study, the coefficient cutoff value of 0.81 (i.e., $r > 0.81$ or $r < -0.81$) was used based on the discrimination significance ($p < 0.05$) determined according to the significance test of the Pearson product-moment correlation coefficient. Classical statistical analysis (one way-ANOVA) was also carried out on some metabolite concentration calculated from eqs 1−3 to confirm the significant differences derived from OPLS-DA using SPSS 13.0 software with a Tukey post-test.

For the LC-UV and LC-MS results, multivariate data analysis was conducted with the same software on the integral areas of some major signals normalized to the weights of extracts, respectively. PCA was conducted using mean-centered data and further analysis was carried out using the OPLS-DA method with unit variance scaled data and plotted in the same fashion as described above.

Results and Discussion

NMR and HPLC-DAD-MS Analysis of SMB Extracts. Figures 2 and 5 show the representative ^{1}H NMR spectra of SMB extracts obtained from four solvents (Figure 2) and from three drying processes (Figure 5). The resonances were assigned to specific metabolites (with both ^{1}H and ^{13}C data tabulated in Table 1) based on the literature data,[40] in-house databases and extensive 2D NMR analysis including ^{1}H−^{1}H COSY, ^{1}H−^{1}H TOCSY, ^{1}H−^{1}H *J*-resolved, ^{1}H−^{13}C HSQC, and ^{1}H−^{13}C HMBC 2D NMR spectroscopy. We also measured the spin−lattice relaxation times for plant metabolites which are, to the best of our knowledge, reported for the first time. These data (Table 2) showed that T_1 values for the same metabolite in different extracts were broadly similar and the most metabolites in the extracts of aqueous hydrophilic solvents had T_1 shorter than 2s. The absolute concentrations of some metabolites were calculated taking the relaxation time into consideration (mean ± standard deviation, mg/g extracts) from five parallel samples (Table 3). It is obvious that raffinose, sucrose and malate were the most abundant primary metabolites (about 290, 18, and 26 mg/g extract, respectively), whereas salvianolic acid B, lithospermic acid and rosmarinic acid were three major polyphenolic acids (about 82, 5, and 4 mg/g extracts, respectively).

LC-DAD-MS profiles for SMB extracts were obtained in the forms of LC-UV (Supporting Information Figures S1 and S6) and LC-MS chromatograms (Supporting Information Figures S2 and S7) with 44 secondary metabolites detected; most of their identities were tentatively assigned based on the literature data[41,42] with the pseudomolecular ions $[M - H]^-$, $[M + Na - 2H]^-$, $[2M - H]^-$, $[M + H]^+$, $[M + Na]^+$, $[M + 2Na - H]^+$, $[2M + Na]^+$, fragment ions and UV absorbance (Supporting Information Table S2). Genipin, umbelliferone, a caffeic acid dimer, 4 prolithospermic acid derivatives and 10 unknown components were reported for the first time in this plant.

The NMR methods detected 37 abundant metabolites including both primary and secondary metabolites, whereas LC-DAD-MS methods detected exclusively the secondary ones, indicating different but complementary information obtained with these two methods. Specifically, NMR methods detected 3 SMB secondary metabolites including salvianolic acid B, lithospermic acid and rosmarinic acid in the aqueous solvent extracts together with 29 primary metabolites including 5 sugars, 10 organic acids and 13 amino acids, which, to the best of our knowledge, were comprehensively reported for the first time. Five diterpenoids were also detected in the chloroform−methanol extracts including tanshinone I, tanshinone IIA, 1,2-dihydrotanshinone I, cryptotanshinone and 15,16-dihydrotanshinone I. In contrast, LC-DAD-MS methods selectively detected 44 SMB secondary metabolites including the eight abundant metabolites detected in NMR spectra and less abundant ones such as danshensu and salvianolic acids. It is

Table 1. NMR Assignments of the Major Metabolites in SMB Extracts[a]

peak	metabolites	assignment	δ^1H (multiplicity)	δ^{13}C	assigned with
1	Isoleucine	δ-CH_3	0.94	14.1	TOCSY, JRES, HSQC
		γ-CH_3	1.01	17.5	
		γ-CH	1.27	19.7	
		γ′-CH	1.47	27.1	
		β-CH	1.97	38.8	
2	Leucine	δ-CH_3	0.96	23.6	TOCSY, JRES, HSQC
		β-CH_2	1.72	42.8	
3	Valine	γ′-CH_3	0.99 (d, 6.9 Hz)	19.6	TOCSY, JRES, HSQC
		γ-CH_3	1.04 (d, 6.9 Hz)	20.9	
		β-CH	2.26	31.9	
4	Threonine	CH_3	1.33 (d, 6.4 Hz)	22.2	TOCSY, JRES, HSQC
		β-CH	4.28	68.9	
5	Lactate	β-CH_3	1.33 (d, 7.0 Hz)	22.2	TOCSY, JRES, HSQC,
		α-CH	4.13	69.6	HMBC
		COOH		185.3	
6	Alanine	β-CH_3	1.49 (d, 7.4 Hz)	19.3	TOCSY, JRES, HSQC,
		α-CH	3.79	53.5	HMBC
		COOH		178.9	
7	γ-aminobutyrate	β-CH_2	1.90	26.7	TOCSY, JRES, HSQC,
		α-CH_2	2.30 (t, 7.5 Hz)	37.2	HMBC
		γ-CH_2	3.01 (t, 7.3 Hz)	42.5	
		COOH		184.5	
8	Acetate	CH_3	1.93 (s)	26.1	JRE, HSQC, HMBC
		COOH		184.2	
9	Proline	γ-CH_2	2.00 (m)	26.5	TOCSY, HSQC, HMBC
		δ′-CH	3.34 (m), 3.42 (m)	49.2	
		β-CH_2	2.34 (m)	31.7	
		α-CH	4.14 (m)	64.1	
		COOH		177.6	
10	Pyroglutamate	γ′-CH	2.04	28.7	TOCSY, HSQC, HMBC
		β-CH_2	2.41	32.5	
		γ-CH	2.51	28.7	
		α-CH	4.18	61.6	
		C═O		185.1	
		COOH		182.5	
11	Glutamine	β-CH_2	2.15 (m)	29.6	TOCSY, HSQC, HMBC
		γ-CH_2	2.45 (m)	33.7	
		α-CH	3.79	57.0	
		COOH		176.8, 181	
12	Malate	β′-CH	2.37	45.9	TOCSY, JRE, HSQC
		β-CH	2.68 (dd, 15.6, 3.5 Hz)	45.9	HMBC,
		α-CH	4.31	73.7	
		COOH		176.3	
13	Succinate	CH_2	2.42 (s)	35.8	JRE, HSQC, HMBC
		COOH		184.5	
14	α-Ketoglutaric acid	β-CH_2	2.45	33.7	TOCSY, JRE, HSQC
		γ-CH_2	3.01 (t, 7.3 Hz)	38.9	
15	Malonate	CH_2	3.13 (s)	#	JRE, HMBC
		COOH		180.2	
16	Choline	$N(CH_3)^+$	3.21 (s)	56.6	TOCSY, JRE, HSQC,
		CH_2OH	4.06	58.2	HMBC
		CH_2N	3.56	70.3	
17	Tartaric acid	CHOH	4.34 (s)	79.1	JRE, HSQC, HMBC
		COOH		181.7	
18	β-Galactose	C_1H	4.59 (d, 7.8 Hz)	99.6	TOCSY, JRE, HSQC
		C_2H	3.50	74.7	HMBC
		C_3H	3.66	76.0	
		C_4H	3.94	72.1	
19	β-Glucose	C_1H	4.65 (d, 7.8 Hz)	99.2	TOCSY, JRE, HSQC
		C_2H	3.26	76.8	HMBC
		C_3H	3.48	74.2	
20	α-Glucose	C_1H	5.24 (d, 3.8 Hz)	95.5	TOCSY, JRE, HSQC
		C_2H	3.55	72.5	HMBC
		C_3H	3.72	69.4	
		C_4H	3.42	72.1	
		C_5H	3.85	71.9	
21	α-Galactose	C_1H	5.27 (d, 3.8 Hz)	95.2	TOCSY, JRE, HSQC
		C_2H	3.83	65.2	HMBC
		C_5H	4.02	72.8	
22	Melibiose	Glc-αC_1H	5.26 (d, 3.8 Hz)	95.0	TOCSY, JRE, HSQC
		Glc-αC_2H	3.55	72.3	HMBC
		Glc-αC_3H	3.72	75.9	
		Glc-αC_5H	4.03	73.0	
		Glc-βC_1H	4.69 (d, 8.0 Hz)	99.0	
		Glc-βC_2H	3.28	77.1	
		Glc-βC_3H	3.50	74.7	
		Glc-βC_4H	3.65	76.2	
23	Sucrose	Glc-C_1H	5.42 (d, 3.8 Hz)	95.0	TOCSY, JRE, HSQC
		Glc-C_2H	3.57	73.7	HMBC
		Glc-C_3H	3.81	75.6	
24	Raffinose	Glc-C_1H	5.44 (d, 3.8 Hz)	95.1	TOCSY, JRE, HSQC
		Glc-C_2H	3.57	72.7	HMBC
		Glc-C_3H	3.77	70.6	
		Glc-C_5H	4.07	74.0	

Table 1. Continued

peak	metabolites	assignment	δ^1H (multiplicity)	δ^{13}C	assigned with
25	Salvianolic acid B	7″-H	2.90 (dd, 14.4, 9.7 Hz)	39.8	TOCSY, JRE, HSQC,
		7″-H	3.10 (dd, 14.4, 3.9 Hz)	39.8	HMBC
		8″-H	5.00 (dd, 9.7, 3.9 Hz)	79.5	
		α-CH═CH	5.87 (d, 16.0 Hz)	118.5	
		β-CH═CH	6.99 (d, 16.0 Hz)	144.7	
		7‴-H	2.98	39.2	
		7‴-H	2.56	39.2	
		8‴-H	4.90	80.6	
		2-H	5.98 (d, 5.6 Hz)	89.5	
		3-H	4.33 (d, 5.6 Hz)	59.5	
		2‴-H	6.24 (d, 2.6 Hz)	119.7	
		5‴-H	6.42 (d, 8 Hz)	119.2	
		6‴-H	6.08 (dd, 8.0, 2.6 Hz)	123.2	
		6″-H	6.76	#	
		5″-H	6.93	#	
		5-H	7.06(d, 8.0 Hz)	#	
		6-H	6.92	#	
26[b]	Cryptotanshinone	H-1	3.22 (t, 6.4 Hz)	30.0	TOCSY, JRE, HSQC
		H-2	1.79 (m)	19.1	HMBC
		H-3	1.66 (m)	37.9	
		H-6	7.62 (d, 8.2 Hz)	120.4	
		H-7	7.49 (d, 8.2 Hz)	122.5	
		H-15	3.60 (m)	34.9	
		H-16α	4.89 (t, 9.5 Hz)	81.6	
		H-16*β*	4.36 (dd, 9.5, 6.0 Hz)	81.6	
		H-17	1.36 (d, 6.8 Hz)	19.0	
		H-18	1.31 (s)	29.5	
		H-19	1.31 (s)	29.5	
27[b]	15,16-dihydrotanshinone I	H-1	9.32 (d, 8.8 Hz)	125.3	TOCSY, JRE, HSQC
		H-2	7.57 (dd, 8.8, 6.9 Hz)	120.5	HMBC
		H-3	7.41 (d, 6.9 Hz)	#	
		H-6	8.32 (d, 8.6 Hz)	132.9	
		H-7	7.79 (d, 8.6 Hz)	120.4	
		H-15	3.66 (m)	35.1	
		H-16α	4.44 (dd, 9.4, 6.3 Hz)	81.7	
		H-16*β*	4.97 (t, 9.4 Hz)	81.7	
		H-17	1.42 (d, 6.8 Hz)	18.9	
		H-18	2.70 (s)	20.0	
28[b]	1,2-dihydrotanshinone I	H-1	3.34 (t, 8.0 Hz)	25.0	TOCSY, JRE, HSQC
		H-2	2.06 (m)	#	HMBC
		H-3	6.05 (m)	#	
		H-18	2.27 (d, 1.2 Hz)	34.4	
29[b]	Tanshinone I	H-1	9.28 (d, 8.8 Hz)	125.0	TOCSY, JRE, HSQC
		H-2	7.57 (dd, 8.8, 6.9 Hz)	130.6	HMBC
		H-3	7.37 (d,6.9 Hz)	128.5	
		H-6	8.32 (d, 8.6 Hz)	132.9	
		H-7	7.86 (d,8.6 Hz)	118.9	
		H-16	7.32 (d, 1.2 Hz)	142.1	
		H-17	2.30 (d,1.2 Hz)	9.1	
		H-18	2.70 (s)	20.0	
30[b]	Tanshinone IIA	H-1	3.19 (t, 6.4 Hz)	30.1	TOCSY, JRE, HSQC
		H-2	1.79 (m)	19.3	HMBC
		H-3	1.66 (m)	37.9	
		H-6	7.63 (d, 8.2 Hz)	133.4	
		H-7	7.54 (d, 8.2 Hz)	120.3	
		H-16	7.22 (d, 1.2 Hz)	141.3	
		H-17	2.26 (d,1.2 Hz)	9.0	
		H-18	1.26 (s)	29.7	
		H-19	1.26 (s)	29.7	
31	*n*-butanol	CH_3-4	0.90 (t, 7.3 Hz)	15.9	TOCSY, JRE, HSQC,
		CH_2-3	1.34 (m)	21.4	HMBC
		CH_2-2	1.54 (q)	33.6	
		CH_2-1	3.56 (t, 6.8 Hz)	73.5	
32[c]	U1		2.25 (d, 3 Hz)	33.2	
33[b]	Linoleic fatty chain ($C18:2\Delta^{9,12}$)	CH_2-2	2.34	33.7	TOCSY, HSQC, HMBC
		CH_2-3	1.63	25.1	
		CH_2-4	1.33	29.7	
		CH_2-8	2.04	27.2	
		CH_2-9	5.35	129.4	
		CH_2-10	5.35	122.0	
		CH_2-11	2.76	26.0	
		CH_2-12, CH_2-13	5.35	128.2	
		CH_3	0.89	13.8	
34[b]	Linoleic fatty chain ($C18:3\Delta^{9,12,15}$)	CH_2-2	2.34	33.7	TOCSY, HSQC, HMBC
		CH_2-3	1.63	25.1	
		CH_2-4	1.31	29.7	
		CH_2-8	2.07	27.2	
		CH_2-9	5.35	128.2	
		CH_2-10	5.35	128.2	
		CH_2-11	2.81	26.0	
		CH_2-12, CH_2-13	5.35	128.2	
		CH_3	0.97	19.5	
35	rosmarinic acid	α-CH═CH	6.34 (d, 16.0 Hz)	#	TOCSY, JRE
		β-CH═CH	7.55 (d, 16.0 Hz)	#	

Table 1. Continued

peak	metabolites	assignment	δ^1H (multiplicity)	δ^{13}C	assigned with
36	Lithospermic acid	α-CH═CH	6.32 (d, 16.0 Hz)	#	TOCSY, JRE
		β-CH═CH	7.70 (d, 16.0 Hz)	#	
37	Formate	H−C═O	8.46 (s)	#	JRE

[a] Multiplicity: singlet (s), doublet (d), triplet (t), doublet of doublets (dd), quintet (q), multiplet (m). U: unidentified signal. #: the signals or the multiplicities were not determined. [b] The signals were only found in the spectra of chloroform−methanol extracts. [c] The signals were found in the spectra of 50% aqueous ethanol extracts.

Table 2. Proton Spin−lattice Relaxation Time (T_1) Values for Some Selected Metabolites

		extracts from different solvents (s)				extracts from drying processes		
	δ (ppm)	A	B	C	D	FD	SD	AD
TSP	0	3.22 ± 0.04	3.12 ± 0.05	3.07 ± 0.03		2.97 ± 0.02	3.21 ± 0.05	3.15 ± 0.02
TMS	0				3.20 ± 0.03			
Isoleucine	1.01 (d)	-	-	-	-	0.89 ± 0.01	0.88 ± 0.004	0.89 ± 0.20
Valine	1.04 (d)	-	-	-	-	0.96 ± 0.16	0.84 ± 0.01	1.06 ± 0.17
Lactate	1.33 (d)	1.56 ± 0.15	1.36 ± 0.18	1.64 ± 0.13	-	0.91 ± 0.18	0.78 ± 0.01	1.10 ± 0.17
Alanine	1.48 (d)	1.5 ± 0.13	1.46 ± 0.18	1.80 ± 0.20	-	0.90 ± 0.01	1.20 ± 0.02	1.23 ± 0.18
Glutamine	2.14	1.06 ± 0.08	1.04 ± 0.18	1.12 ± 0.18	-	1.00 ± 0.13	0.98 ± 0.005	1.12 ± 0.07
Succinate	2.41 (s)	2.37 ± 0.03	2.54 ± 0.07	2.41 ± 0.02	-	2.45 ± 0.10	2.36 ± 0.10	2.40 ± 0.06
Malate	2.68 (dd)	1.02 ± 0.07	1.11 ± 0.15	1.01 ± 0.05	-	1.01 ± 0.17	0.93 ± 0.02	1.26 ± 0.15
Sucrose	5.41 (d)	0.98 ± 0.19	1.02 ± 0.10	1.26 ± 0.22	-	1.07 ± 0.12	1.12 ± 0.01	1.02 ± 0.13
Raffinose	5.43 (d)	0.92 ± 0.05	0.88 ± 0.07	0.84 ± 0.06	-	0.96 ± 0.18	0.93 ± 0.01	0.90 ± 0.06
Salvianolic acid B	7.03 (d)	1.53 ± 0.13	1.25 ± 0.02	1.37 ± 0.08	-	1.80 ± 0.26	1.40 ± 0.01	1.74 ± 0.10
Tanshinone I	9.28 (d)	-	-	-	3.02 ± 0.01	-	-	-
15,16-dihydrotanshinone I	9.32 (d)	-	-	-	5.22 ± 0.01	-	-	-
Cryptotanshinone	3.22 (t)	-	-	-	0.90 ± 0.03	-	-	-
Tanshinone IIA	3.19 (t)	-	-	-	0.85 ± 0.01	-	-	-
1,2-dihydrotanshinone I	3.34 (t)	-	-	-	1.25 ± 0.02	-	-	-

[a] A, B, C, and D denote SMB extracts from boiling water, 50% aqueous ethanol, 50% aqueous methanol, and chloroform−methanol (v/v, 3/1), respectively; FD, SD, and AD denote freeze-drying, sun-drying, and air-drying, respectively. -: T_1 was not determined due to weakness or overlapping of signals.

Table 3. The Correlation Coefficients from OPLS-DA and the Metabolites Content of SMB Extracts from Different Solvents

	coefficient[a]			mean ± SD[b] (mg/g)			
metabolite	A/B[c]	B/C	C/A	A	B	C	D
Lactate	0.981	−0.967	0.583	1.14 ± 0.03[d]	2.43 ± 0.09[e]	1.28 ± 0.01	-
Pyroglutamate	−0.955	−0.403	−0.908	-	-	-	-
Glutamine	0.836	0.355	0.854	14.45 ± 0.76[d]	16.37 ± 0.94	17.30 ± 0.58[f]	-
Succinate	0.966	−0.437	0.868	4.96 ± 0.29[d]	6.04 ± 0.27	5.83 ± 0.25[f]	-
Malate	−0.587	−0.794	−0.485	26.30 ± 0.74	26.21 ± 0.99	26.10 ± 0.83	-
α-Ketoglutaric acid	−0.954	−0.433	−0.869	-	-	-	-
Glucose	−0.630	0.452	−0.231	-	-	-	-
Melibiose	0.525	−0.641	0.347	-	-	-	-
Galactose	−0.155	0.289	0.062	-	-	-	-
Sucrose	0.149	0.122	0.290	17.77 ± 1.48	18.93 ± 2.86	21.25 ± 2.13	-
Raffinose	−0.546	0.376	0.415	293.42 ± 17.38	290.67 ± 12.16	311.14 ± 11.93	-
Rosmarinic acid	0.196	0.370	0.314	4.19 ± 0.35	4.30 ± 0.68	4.66 ± 0.52	-
lithospermic acid	−0.683	0.169	−0.680	5.03 ± 0.34	4.45 ± 0.64	4.77 ± 0.30	-
Salvianolic acid B	−0.598	0.650	0.358	83.88 ± 3.23	81.79 ± 4.27	87.08 ± 5.93	-
Tanshinone I	-	-	-	-	-	-	7.06 ± 0.67
15,16-dihydrotanshinone I	-	-	-	-	-	-	4.30 ± 0.54
Cryptotanshinone	-	-	-	-	-	-	7.12 ± 1.44
Tanshinone IIA	-	-	-	-	-	-	15.41 ± 2.18
1,2-dihydrotanshinone I	-	-	-	-	-	-	7.90 ± 1.34

[a] The coefficients from OPLS-DA results, positive and negative signs indicate positive and negative correlation in the concentrations, respectively. The coefficient of 0.81 was used as the cutoff value for the significant difference evaluation ($p < 0.05$). [b] The absolute concentration and standard deviation (mean ± SD, mg/g the SMB extracts) obtained from five parallel samples. [c] A, B, C and D denote SMB extracts from boiling water, 50% aqueous ethanol, 50% aqueous methanol, and chloroform−methanol (v/v, 3/1), respectively. The significant difference by one-way ANOVA analysis ($p < 0.05$). -: The absolute concentration is not determined due to signal weakness or overlapping. [d] A vs B. [e] B vs C. [f] A vs C.

interesting to note that, with the present methods, two different chromatographic regions are clearly present for polyphenolic acids (RT ∼2−40 min) and diterpenoids (RT > 40 min). MS detections were apparently biased for different class of metabolites with polyphenolic acids detected in both the negative and positive ion modes and diterpenoids mainly in the positive modes. For example, the LC-MS profiles for the air-dried extracts showed salvianolic acid B (peak 10) as the most abundant peak in the negative mode (Supporting Information Figure S7b), whereas cryptotanshinone (peak 24) as the most

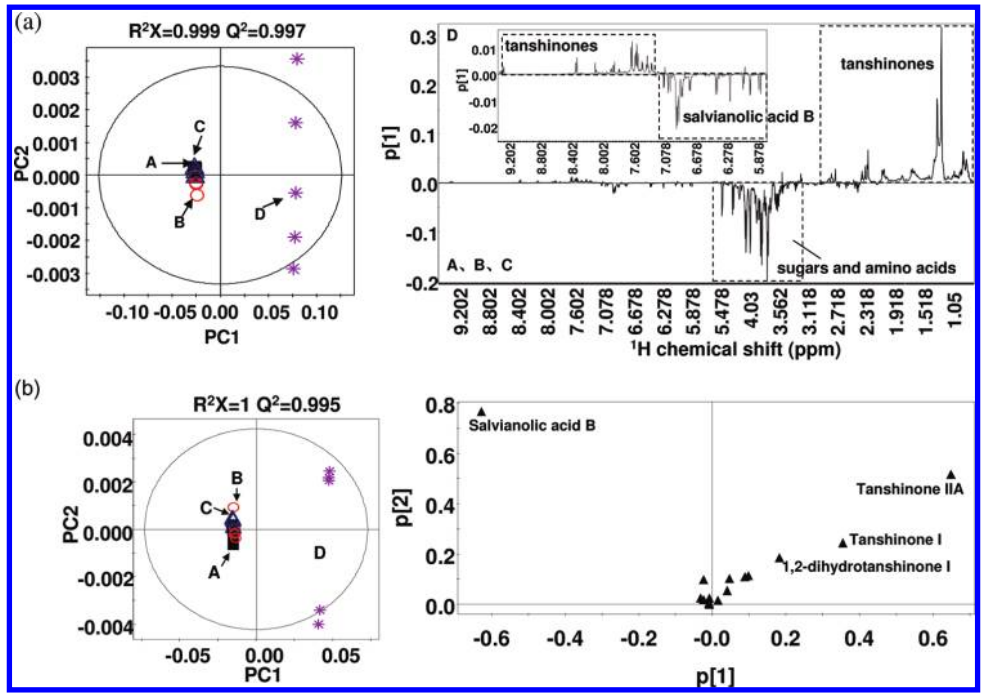

Figure 3. PCA scores plots (left) and corresponding loadings plots (right) derived from (a) NMR and (b) LC-UV data (280 nm) for SMB extracts obtained from (A) boiling water (black ■), (B) 50% aqueous ethanol (red ○), (C) 50% aqueous methanol (blue Δ) and (D) chloroform−methanol (v/v, 3/1) (purple *).

abundant peak in the positive mode (Supporting Information Figure S7a); for the aqueous extracts, few peaks for diterpenoids (RT > 40 min) were observable in the negative mode (Supporting Information Figure S2b), whereas such peaks were clearly visible in the positive ionization mode (Supporting Information Figure S2a). The reverse-phase LC-DAD-MS showed almost no peaks from the primary metabolites (Supporting Information Figures S1, S2, S6 and S7).

SMB Metabolite Composition Variations with Extraction Solvents. Understanding the solvent dependence of metabolite compositions of plant extracts is fundamentally important since solvent extraction is a matter of necessity for the plant metabonomic analysis. Visual inspection of the ^{1}H NMR spectra (Figure 2) revealed obvious differences between metabolite profiles of the SMB extracts obtained from the hydrophilic solvents (A, B, and C) and that from the hydrophobic solvent (D). While SMB extracts from three hydrophilic solvents (A−C) were dominated by sugars, amino acids, organic acids and polyphenolic acids, the chloroform−methanol (D) extracts contained mainly diterpenoids such as 1,2-dihydrotanshinone I, 15,16-dihydrotanshinone I, tanshinone I and cryptotanshinone (Figure 2). The LC-UV profiles at 280 nm (Supporting Information Figure S1) and LC-MS results (Supporting Information Figure S2) only showed secondary metabolites, among which polyphenolic acids especially salvianolic acids are dominant in extracts from hydrophilic solvents (A−C), whereas the methanol−chloroform extracts were dominated by diterpenoids (RT > 40 min). This observation further suggested that the chloroform−methanol mixture employed in this study is an excellent solvent system for selective extraction of diterpenoids or tanshinones. However, the complexity of SMB metabolite composition makes it prohibitively difficult to analyze these data in details by visual comparison alone. Multivariate data analyses are much more efficient in such cases.

The PCA scores plot of NMR data (Figure 3a, left) showed clear differences between extracts obtained from hydrophilic solvents (A−C) and the solvent (D) in the first two principal components (PC1 and PC2), which cumulatively explained 99.9% of all variables ($R^2X = 0.999$, $Q^2 = 0.997$). The metabolite composition of SMB extracts from three hydrophilic solvents was more similar than that of chloroform−methanol extracts. The corresponding loadings plot (Figure 3a, right) showed that, compared with extracts from three hydrophilic solvents, chloroform−methanol extracts contained more diterpenoids such as tanshinone I, 15,16-dihydrotanshinone I, 1,2-dihydrotanshinone I and cryptotanshinone but less sugars, amino acids and salvianolic acid B. The samples from chloroform−methanol were more scattered probably because of high volatility of these solvents resulting in some variations in solvent composition. The LC-UV results (Figure 3b) agreed with these findings.

Pair-wise comparative OPLS-DA results of NMR data (Figure 4) showed significant metabonomic differences between SMB extracts from three aqueous solvents with the values of R^2X and Q^2 indicating good qualities for these models. The metabolites contributed significantly to the classifications were obtained (Table 3) based on the discrimination significance ($p < 0.05$). The results (Figure 4, Table 3) showed that compared with the hot-water extracts, aqueous ethanol extracts contained more lactate, succinate and glutamine but less pyroglutamate and α-ketoglutarate. Aqueous methanol extracts contained more glutamine and succinate but less pyroglutamate and α-ketoglutarate (Figure 4, Table 3) than boiling water extracts. Higher levels of lactate were also present in aqueous ethanol extracts than in aqueous methanol ones. No significant differences were observed in the concentration of rosmarinic acid, lithospermic acid and salvianolic acid B in the extracts from three hydrophilic solvents. Such compositional differences were probably derived from extraction efficiency or solubility differences rather than enzymic changes since these solvents are expected to suppress enzyme activities. Although subtle differences are present, the 50% aqueous methanol is probably the best solvent for the purpose of postextraction handling and

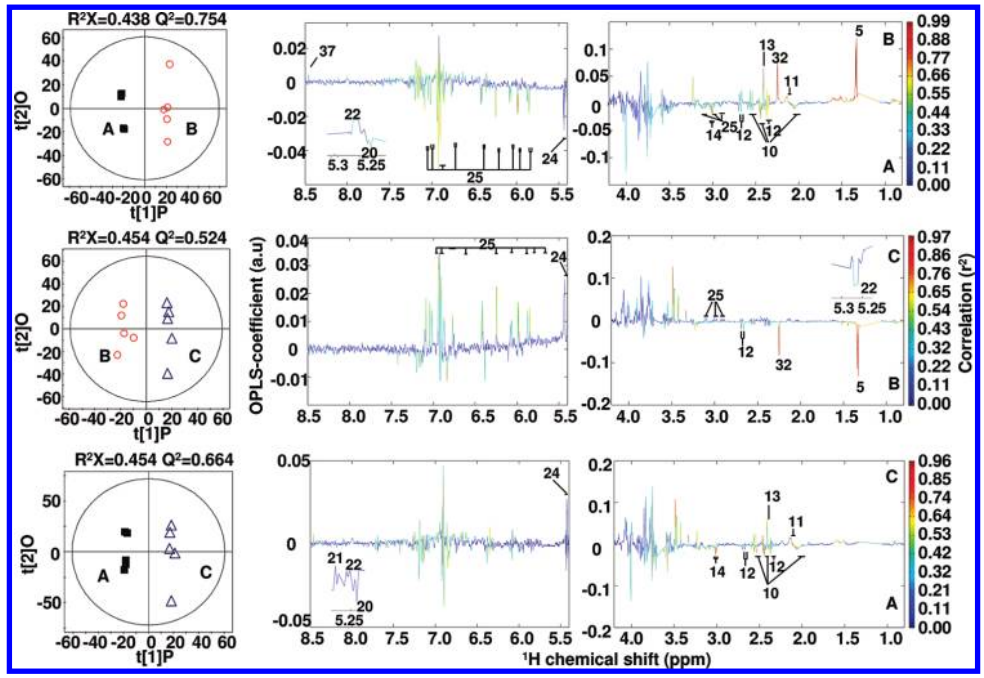

Figure 4. OPLS-DA scores (left) and coefficient-coded loadings plots (right) derived from NMR data for SMB extracts obtained from (A) boiling water (black ■), (B) 50% aqueous ethanol (red ○), (C) 50% aqueous methanol (blue Δ) (see Table 1 for metabolite identification key).

direct employment of deuterated solvents (to eliminate the solvent removal step). The absolute concentrations of metabolites were also subjected to classical statistical analysis (one-way ANOVA) and the results were consistent with the OPLS-DA ones.

Furthermore, the LC-UV peak areas of 16 components were employed to analyze the potential differences for the SMB secondary metabolites including 6 polyphenolic acids, namely, danshensu, rosmarinic acid, lithospermic acid, salvianolic acid B, salvianolic acid B isomer and salvianolic acid L, and 8 tanshinones, namely, tanshinone IIB, trijuganone C, trijuganone B, 15,16-dihydrotanshinone I, cryptotanshinone, tanshinone I, 1,2-dihydrotanshinone I and tanshinone IIA. PCA and OPLS-DA were conducted on the LC-UV profiles scaled to the weight of extracts assuming that the molar extinction coefficient for the same metabolite in different extracts was not drastically different. The OPLS-DA results (Supporting Information Figure S3) showed significant intergroup differences in the secondary metabolite composition of the extracts obtained from the hydrophilic solvents with the corresponding R^2X/Q^2 values confirming the good model qualities. Detailed coefficient analysis revealed that, compared with boiling water extracts, the extracts from both aqueous ethanol and methanol contained significantly higher levels of diterpenoids ($p < 0.05$) including tanshinone I (peak 25), tanshinone IIA (peak 27), tanshinone IIB (peak 15), 15,16-dihydrotanshinone I (peak 21), cryptotanshinone (peak 24), trijuganone B (peak 23) and 1,2-dihydrotanshinone I (peak 26). Aqueous ethanol extracts also contained more salvianolic acid B isomer (peak 11) than water extracts. The ethanol extracts contained statistically higher concentration of tanshinone I than the methanol extracts probably due to the solubility differences in two solvents. No significant differences were observed for the three major polyphenolic acids, that is, rosmarinic acid (peak 8), lithospermic acid (peak 9) and salvianolic acid B (peak 10), which broadly agreed with the NMR results. LC-UV approach detected more polyphenolic acids and tanshinones in the extracts from the hydrophilic solvents which were not observable in NMR spectra suggesting the complementary nature of these two analytical methods.

Moreover, the LC-MS peak areas of 5 components in the negative ion mode and 27 components in the positive ion mode were also employed to analyze the potential differences in extracting the SMB secondary metabolites using different solvents. PCA (Supporting Information Figure S4) and OPLS-DA (Supporting Information Figure S5) were applied to LC-MS profiles with normalization to the weight of extracts, assuming MS response in the same ion mode was not drastically different for the same metabolite in different extracts. OPLS-DA results of LC-MS profiles in the negative ion mode (Supporting Information Figure S5a) showed that aqueous ethanol and aqueous methanol contained significantly higher levels of salvianolic acid B isomer (peak 11) in comparison with the boiling water extracts. OPLS-DA results of LC-MS profiles in the positive ion mode (Supporting Information Figure S5b) showed that, compared with boiling water extracts, aqueous ethanol extracts contained significantly higher levels of genipin (peak 1), and diterpenoids including tanshinone IIB (peak 15), 1-ketoisocryptotanshinone (peak 16), trijuganone C (peak 18), tanshinaldehyde (peak 20), 15,16-dihydrotanshinone I (peak 21), trijuganone B (peak 23), cryptotanshinone (peak 24), tanshinone I (peak 25), 1,2-dihydrotanshinone I (peak 26) and tanshinone IIA (peak 27). In addition, 5 unknown components (peak 2, 3, and 5−7) and prolithospermic acid derivatives also had higher concentration in ethanol extracts. Similar observation was made for the aqueous methanol extracts, although levels of genipin and peak 2−5 were not statistically significant. Aqueous ethanol was capable of extracting more 15,16-dihydrotanshinone I (peak 21) and tanshinone I (peak 25) than aqueous methanol. The LC-MS results broadly agreed with the NMR and LC-UV results. It is worth-noting that the MS responses of metabolites are dependent on ionization modes.

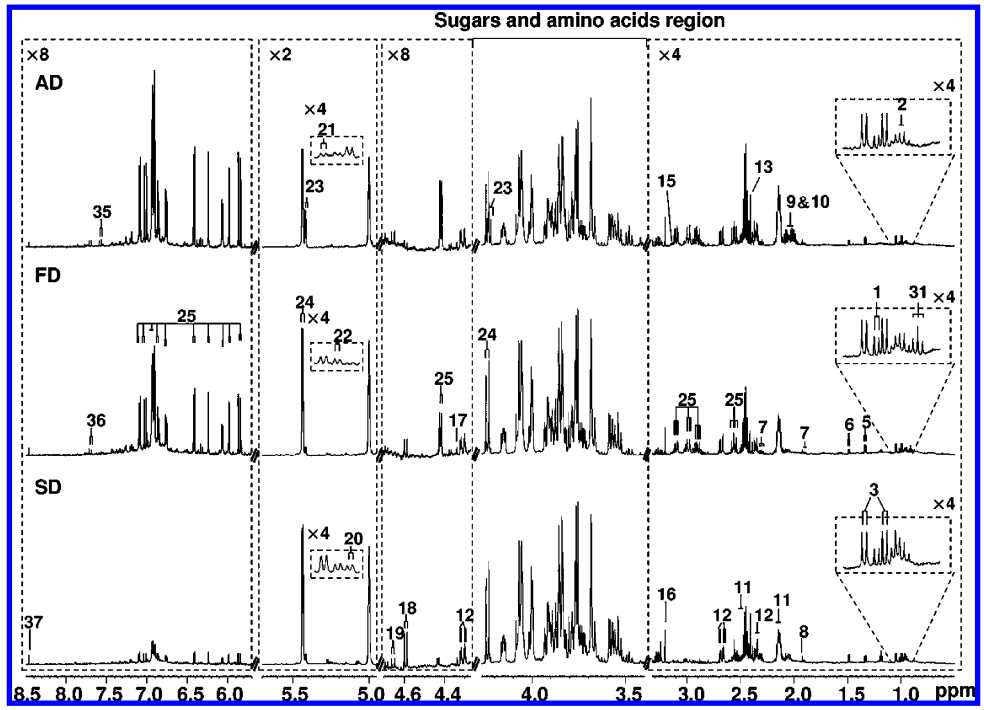

Figure 5. The 600 MHz ^{1}H NMR spectra of extracts derived from freeze-dried (FD), air-dried (AD) and sun-dried (SD) SMB. The spectral regions were expanded 4 times for δ3.22−0.50, 2 times for δ5.70−4.95 and 8 times for δ4.70−4.28 and δ8.50−5.70 (see Table 1 for metabolite identification key).

While polyphenolic acids have good MS responses in both the positive and negative ionization modes, diterpenoids (tanshinones) have much better responses in the positive ion mode. Polyphenolic acids often showed their quasi-molecular ions of $[M - H]^-$, $[M + Na - 2H]^-$ and $[2M - H]^-$ in the negative mode and $[M + H]^+$, $[M + Na]^+$ and $[M + 2Na - H]^+$ in the positive mode, whereas diterpenoids only showed the above quasi-molecular ions in the positive mode.

It is well-known that the NMR signal intensities of metabolites have excellent correlation with their concentration. However, such correlation is not available for the LC-MS signals. For example, in the same aqueous methanol extract, the concentrations of salvianolic acid B, rosmarinic acid and lithospermic acid were about 121.2, 12.9, and 8.9 (μmol/g extract), respectively. The LC-MS profiles of the same extracts (Supporting Information Figure S2) showed that the intensity ratios for rosmarinic acid (peak 8) and lithospermic acid (peak 9) were about 1:1 and 3:1 in the positive (Supporting Information Figure S2a) and negative ion modes (Supporting Information Figure S2b), respectively, which was markedly different from their molar ratios (about 4:3, Table 3).

Such discrepancies are even more striking for different metabolites in the same extract. In aqueous methanol extracts, for instance, the peak ratios for cryptotanshinone (peak 24) and salvianolic acid B (peak 10) were about 1:3 in the positive (Supporting Information Figure S2a, C) and 1:79 in the negative MS modes (Supporting Information Figure S2b, C) even though their concentration ratio was about 1:13; in the chloroform−methanol extracts, the peak ratios for cryptotanshinone and salvianolic acid B were about 217:1 in the positive mode (Supporting Information Figure S2a, D), whereas peaks for these two metabolites were not clearly visible in the negative mode (Supporting Information Figure S2b, D). These observations suggest that in the LC-MS profiles the metabolite intensities vary drastically with the MS conditions probably due to variable ionization efficiency. Therefore, extra care and justifications should be considered when normalizing the LC-MS data to the sum of profile intensities as presently employed in many LC-MS based metabonomics studies.

Water Depletion Induced Metabonomic Alterations to SMB Roots. To understand the effects of drying-induced osmotic stresses on the SMB metabolism, three different drying processes were employed with freeze-drying as control, air-drying and sun-drying as drying-stressors. Both ^{1}H NMR spectra (Figure 5) and LC-DAD-MS data (Supporting Information Figures S6 and S7) showed clear differences between the metabolite profiles of SMB extracts obtained from three different drying processes. NMR spectra (Figure 5) revealed obvious differences in the peak intensities for proline, sucrose and salvianolic acid B, whereas marked intensity differences in peak 22 (m/z 359 in the positive ion mode), rosmarinic acid (peak 8), lithospermic acid (peak 9) and salvianolic acid B (peak 10) were noticeable in the LC-MS profiles (Supporting Information Figure S7) for samples from the three different drying processes. This implies that the SMB metabonomic responses to drying-induced stresses involve both its primary and secondary metabolites, which is in good agreement to what has been observed for rosemary.[31]

The PCA scores plots generated from NMR data (Figure 6a) and LC-UV profiles of the SMB extracts (Figure 6b) showed clear separation for the SMB extracts from different drying methods with tight intragroup clustering, indicating good reproducibility in both extraction and data acquisitions. Pairwise comparative OPLS-DA results confirmed the significant intergroup differences in scores plots (Figure 7, left) for extracts from the three different drying treatments. The correlation coefficients of metabolites having statistically significant contributions to the differences ($p < 0.05$) were tabulated in Table 4 together with some metabolites' concentration (mean ± SD, mg/g extracts). These results revealed that, compared with

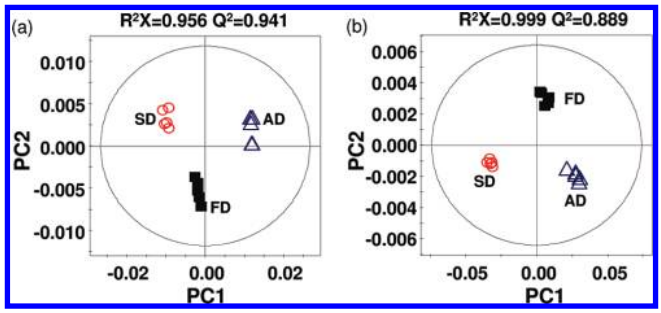

Figure 6. PCA scores plots derived from (a) NMR and (b) LC-UV data (280 nm) for extracts obtained from freeze-dried (FD, black ■), sun-dried (SD, red ○) and air-dried (AD, blue Δ) SMB roots, respectively.

freeze-drying, air-drying led to significant elevation for proline, glutamine, alanine, succinate and sucrose but alleviation for *n*-butanol, lactate, isoleucine, leucine, valine and raffinose. In comparison to freeze-drying, sun-drying caused significant accumulation of proline, alanine, succinate, leucine, melibiose and raffinose accompanied with depletion of *n*-butanol, lactate, glutamine, malate and salvianolic acid B. Sun-dried samples contained higher levels of alanine, leucine, galactose and raffinose but lower levels of lactate, proline, glutamine, succinate, malate, sucrose and salvianolic acid B than the air-dried samples. The absolute concentrations of metabolites were also subjected to ANOVA and similar conclusions were obtained.

These metabonomic alterations are probably related to the metabolic responses of SMB plant cells to water-depletion stress resulting from the different drying processes. During the freeze-drying process, plant tissues are in the solid state and the plant cells are unable to make swift adjustments in metabolic enzyme activities owing to the lack of water availability (assuming that snap-frozen in liquid nitrogen is fast enough). However, during air- and sun-drying processes, gradual water depletion will lead to steady drought stresses to the plant cells and induce metabolic changes due to the drought adaptation of the plant cells. The accumulation of the proline and sucrose during air-drying and sun-drying (compared to freeze-drying) is in good accordance with the previous findings for plant cells when subjected to drought stresses.[4,43] Under drought stress, proline functions as a compatible osmolyte, storage for carbon and nitrogen,[44] scavenger for reactive oxygen species (ROS)[45] and regulator for intracellular pH. Such response is probably related to the promotion of glutamate-mediated proline biosynthesis under osmotic stress[46] and to the transcriptional activation of the gene encoding pyrroline-5-carboxylate synthase, which is the key regulatory and rate-limiting enzyme in the proline biosynthetic pathway.[47−49] The first enzyme in the pathway of proline degradation, proline dehydrogenase, may also be implicated in the control of free proline levels during the abiotic stress response.[50]

The marked changes of in the levels of sucrose indicated the drought induced effects on photosynthesis and carbohydrate metabolisms, which is in good agreement with previous findings in other plants.[51−53] Sucrose is the key form of photosynthetic and nonphotosynthetic carbon translocation in plant cells and can be synthesized either from fructose-6-phosphate and UDP-glucose with sucrose phosphate synthase or from reversible conversion of fructose and UDP-glucose with sucrose synthase. Sucrose accumulation observed here is therefore consistent with the findings on drought-induced changes in these enzymes activities in plants.[51−53] The alterations in the levels of other amino acids such as isoleucine, leucine, valine and alanine indicated the drying-induced alterations in protein biosynthesis/degradation.[54] The changes in the levels of lactate and the TCA cycle intermediates (e.g., malate and succinate) indicate the alterations in both aerobic and anaerobic glycolysis induced by the osmotic stress.

Furthermore, the raffinose levels decreased during the air-drying process but increased during the sun-drying process. These are probably attributable to the effects of drying speed on enzyme activities and thus the different mode of plant cell responsive actions. Such different metabolic responses have already been observed in *Lolium perenne* and *Arabidopsis thaliana*[55,56] and germinated radicles of cucumber at different growth stages[57] even though no reports have been published on the plant metabonomic responses to rapid and lasting drought stresses on SMB. The drying-induced level changes for salvianolic acid B are related to alterations in shikimate-mediated polyphenol biosynthesis and indicate that plant cells are capable of mobilizing its secondary metabolism (i.e., all possible tools available) in order to prevent ROS injuries under severe water depletion stresses (e.g., drying). Such responses of plant secondary metabolism to water-depletion stress have largely been ignored so far. The different responses of salvianolic acid B biosynthesis to air-and sun-drying processes suggest the functional complexity of plant secondary metabolism in self-protection and perhaps lack of specificity of such biosynthesis to stressors. The details in such mode of actions and the metabolic pathways associated with the rate of water depletion clearly warrant further thorough investigation especially in the levels of transcriptional regulations and protein expressions. However, such investigation is well beyond the scope of the current study and the present results already indicate that NMR-based metabonomics technology is a useful tool to investigate the stress-induced changes in the plant physiology.

To focus on the effects of drying stresses on the secondary metabolism, we also analyzed the changes of 18 most prominent secondary metabolites of SMB detected with LC-UV methods including 10 polyphenolic acids and 8 tanshinones. The OPLS-DA results (Supporting Information Figure S8) showed that, compared with freeze-dried samples, air-dried samples contained significantly higher levels of oligomeric caffeic acids and tanshinones but lower levels of caffeic acid; in contrast, the sun-dried samples had significantly higher levels of tanshinone IIA and 15,16-dihydrotanshinone I but lower levels of polyphenolic acids than the freeze-dried ones. The sun-dried samples contained significant lower levels of polyphenolic acids (e.g., rosmarinic acid and salvianolic acid B) and tanshinones than the air-dried ones. These results suggest that the slow water-depletion induced stress (air-drying) promoted biosyntheses of tanshinones and polyphenolic acids to act as ROS scavengers whereas sun-drying stress promoted the biosynthesis of tanshinones (though to the less extent than air-drying) but suppressed the biosynthesis of the polyphenolic acids. Such sun-drying induced suppression to total phenolic contents has been reported for *P. amarus*,[33] *E. uniflora*[34] and ginger species,[35] although no details on specific phenolic compounds and mechanisms were provided. We speculated that, in the case of sun-drying, light and thermal stress may also play some roles in inducing the aforementioned metabolic changes. Literature search indicates that so far there are no published studies on the drying-induced metabonomic

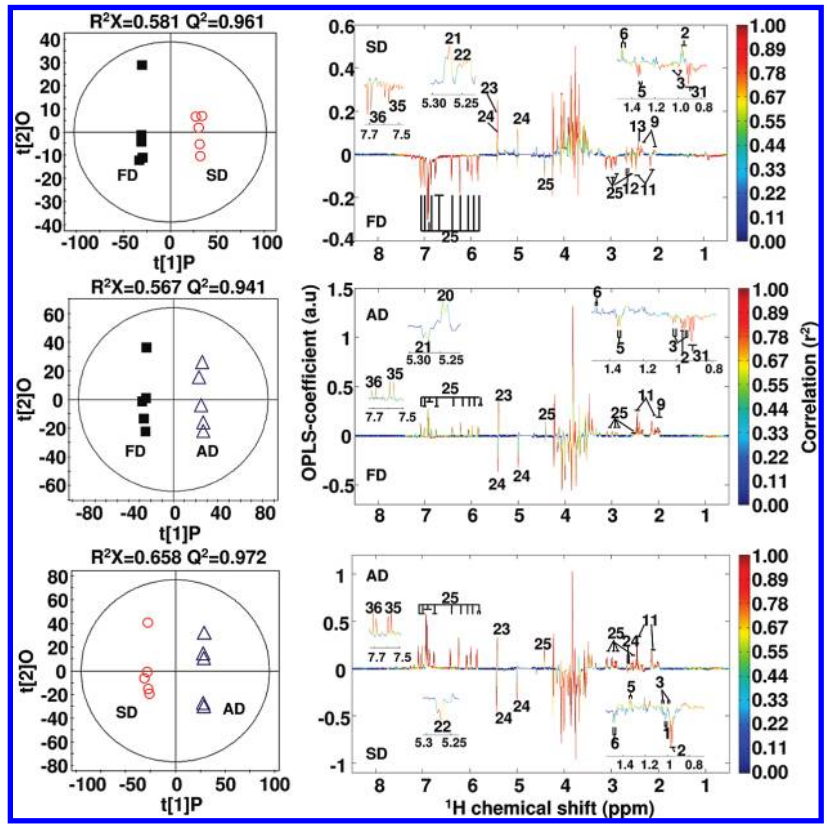

Figure 7. OPLS-DA scores (left) and coefficient-coded loadings plots (right) derived from NMR data for SMB extracts obtained from freeze-dried (FD, black ■), sun-dried (SD, red ○) and air-dried (AD, blue Δ) SMB roots, respectively (see Table 1 for metabolite identification key).

Table 4. The Correlation Coefficients from OPLS-DA and the Metabolites Content of SMB Extracts from Different Drying Processes

	coefficient			mean ± SD (mg/g)		
metabolite	FD vs SD[a]	FD vs AD	SD vs AD	FD	SD	AD
n-butanol	−0.994	−0.993	0.664	-	-	-
Isoleucine	−0.700	−0.952	−0.759	1.06 ± 0.06	1.01 ± 0.09[e]	0.94 ± 0.01
Leucine	0.807	−0.988	−0.988	-	-	-
Valine	−0.892	−0.822	0.699	1.46 ± 0.05[d]	1.20 ± 0.07[e]	1.30 ± 0.03
Lactate	−0.980	−0.963	0.951	1.30 ± 0.06[d]	0.95 ± 0.02[e]	1.18 ± 0.02[f]
Alanine	0.916	0.839	−0.845	0.76 ± 0.03[d]	0.94 ± 0.02[e]	0.82 ± 0.01[f]
Proline	0.892	0.984	0.918	-	-	-
Glutamine	−0.975	0.990	0.996	32.90 ± 0.89[d]	27.71 ± 1.37[e]	47.28 ± 1.87[f]
Succinate	0.956	0.951	0.957	1.68 ± 0.27[d]	2.54 ± 0.17[e]	3.05 ± 0.04[f]
Malate	−0.992	0.466	0.982	15.21 ± 0.55[d]	12.43 ± 0.29	15.39 ± 0.75[f]
Glucose	0.795	0.691	0.370	-	-	-
Melibiose	0.848	0.283	−0.705	-	-	-
Galactose	0.514	−0.710	−0.901	-	-	-
Sucrose	0.507	0.993	0.997	23.98 ± 0.94	26.01 ± 1.79[e]	75.18 ± 3.41[f]
Raffinose	0.956	−0.995	−0.991	398.94 ± 12.91[d]	436.92 ± 30.40[e]	321.13 ± 17.16[f]
Rosmarinic acid	−0.962	0.903	0.970	5.02 ± 1.24[d]	1.80 ± 0.54[e]	7.06 ± 1.04[f]
lithospermic acid	−0.986	−0.818	0.994	7.89 ± 0.69[d]	3.17 ± 0.49	8.70 ± 1.01[f]
Salvianolic acid B	−0.955	0.893	0.965	113.99 ± 10.17[d]	28.68 ± 2.25[e]	130.00 ± 11.47[f]

[a] FD, SD and AD denote freeze-drying, sun-drying and air-drying, respectively. The significant difference by one-way ANOVA analysis ($p < 0.05$). -: The absolute concentration is not determined due to signal weakness or overlapping. [b] The coefficients from OPLS-DA results, positive and negative signs indicate positive and negative correlation in the concentrations, respectively. The coefficient of 0.81 was used as the cutoff value for the significant difference evaluation ($p < 0.05$). [c] The absolute concentration and standard deviation (mean ± SD, mg/g the SMB extracts) were obtained from five parallel samples. [d] FD vs SD. [e] FD vs AD. [f] SD vs AD.

changes for *S. miltiorrhiza* Bunge and the results of this study strongly suggest the importance of secondary metabolisms in the plant adaptation to osmotic stresses, which so far has not been fully considered in the literature.

The LC-MS peak areas (normalized to the weight of extracts) of 14 components in the negative ion mode and 26 components in the positive ion mode (see Supporting Information Figures S9, S10 and Table S2 for details) were further subjected to PCA and OPLS-DA to analyze the secondary metabolism responses to different drought stresses. The PCA model (Supporting Information Figure S9) of the negative and positive ion modes showed clear separation with first two principal components

and tight clustering for each group. OPLS-DA (Supporting Information Figure S10) illustrated clear differentiation in the secondary metabolite composition of the extracts resulting from osmotic stresses with the values of R^2X/Q^2 indicating the good model qualities. In the negative ion mode (Supporting Information Figure S10a), compared to freeze-dried samples, air-dried samples showed significant level elevations for rosmarinic acid (peak 8), salvianolic acid B (peak 10), salvianolic acid L (peak 12), caffeic acid dimer (peak 42), tormentic acid (peak 28) and miltipolone (peak 32) but alleviation of caffeic acid (peak 34), salvianolic acid J (peak 37), salvianolic acid H/I (peak 39) and three unidentified prolithospermic acid derivatives (peak 38, 40 and 41); sun-dried samples contained significant lower levels of polyphenolic acids and tormentic acid (peak 28) than the freeze-dried samples. In the positive mode (Supporting Information Figure S10b), compared with freeze-dried samples, air-dried samples showed significant higher levels of rosmarinic acid (peak 8), salvianolic acid L (peak 12), caffeic acid dimer (peak 42), 1-ketoisocryptotanshinone (peak 16), trijuganone C (peak 18), tanshinaldehyde (peak 20), 15,16-dihydrotanshinone I (peak 21), cryptotanshinone (peak 24) tanshinone IIA (peak 27) and β-sitosterol (peak 19) but lower amounts of umbelliferone (peak 36), the compound at m/z 359 (peak 22), salvianolic acid H/I (peak 39) and three unidentified salvianolic acid derivatives (peak 38, 40 and 41); sun-dried samples contained higher levels of tanshinones and umbelliferone (peak 36) but lower levels of polyphenolic acids. In addition, sun-dried samples contained more umbelliferone (peak 36), tanshinone I (peak 25) and 1,2-dihydrotanshinone I (peak 26) but less polyphenolic acids, trijuganone C (peak 18), β-sitosterol (peak 19), tanshinaldehyde (peak 20) and peak 22 (m/z 359) than air-dried ones. These results imply that air-drying of SMB promotes the biosynthesis of the abundant oligomeric caffeic acids and tanshinones whereas sun-drying suppresses the biosynthesis of polyphenolic acids, which is consistent with the results obtained from NMR analysis. More details in the biosynthetic pathways of these polyphenolic acids and tanshinones are in clear demand to assist our further understandings to such secondary metabolism responses to the drought stresses.

Furthermore, advantages and limitations of two main stream metabonomic analytical approaches (NMR and LC-DAD-MS) are again highlighted in this particular case. NMR results had excellent correlation between the metabolite signal intensities and their concentrations for the abundant metabolites, whereas such correlations were not always readily available in the LC-DAD-MS results. For example, in the air-dried extracts, three metabolites, raffinose, sucrose, and glutamine, were among the most abundant ones with their contents of about 321, 75, and 47 mg/g extract, respectively. The LC-DAD-MS profiles (Supporting Information Figures S6 and S7), however, did not show their peaks at all probably due to their inefficient chromatographic retention and weak responses to both DAD and MS detectors. Instead, the most intense peaks were from salvianolic acid B in the negative MS mode (peak 10, Supporting Information Figure S7b) and cryptotanshinone in the positive mode (peak 24, Supporting Information Figure S7a).

Inconsistencies are also present for the relative MS signal intensities of different metabolites in positive and negative ion modes. In the air-dried SMB samples, the molar ratio for salvianolic acid B and cryptotanshinone was larger than 30:1, whereas their peak ratio was 2:7 in the positive ionization mode (Supporting Information Figure S7a). Even for the same type metabolites (polyphenolic acids), the peak ratios for salvianolic acid B (peak 10) and lithospermic acid (peak 9) were about 9:1 and 25:1 in the positive (Supporting Information Figure S7a) and negative modes (Supporting Information Figure S7b), respectively, although their concentration ratio was about 12:1. This strongly suggests yet again that extra care and justification are absolutely necessary during data normalization when LC-DAD-MS methods are employed in metabonomics studies. In such cases, *in situ* calibrations with reference standards are probably necessary though tedious. Moreover, the selective nature of LC-MS methods in the metabonomic analysis also requires careful consideration in interpreting the biochemical pathways in the holistic manner. Nevertheless, it is worthnoting that LC-DAD-MS methods offer vital complementary information for many low concentration secondary metabolites which otherwise are not detectable in NMR methods (e.g., cryptotanshinone).

Conclusion

This study has unambiguously shown that the combination of NMR and LC-DAD-MS is a much more efficient way for holistic plant metabonomic analysis by providing complementary information. NMR indiscriminately detects the abundant metabolites simultaneously and quantitatively, whereas LC-DAD-MS selectively detects some metabolites, at best, semi-quantitatively without calibrations. The metabonome of SMB roots is largely dominated by 29 primary metabolites, including 5 sugars, 10 carboxylic acids and 13 amino acids, and 8 secondary metabolites including 3 polyphenolic acids and 5 diterpenoids. For metabonomic analysis, the concentration of different metabolites varies with the extraction solvents employed and the choice of extraction solvents for a given biological system requires careful consideration and comparative optimization. For SMB, aqueous methanol is overall a good solvent whereas chloroform/methanol is an excellent solvent system for the selective extraction of the SMB diterpenoids. With results consistent with what was obtained from absolute metabolite concentrations, the efficiency of OPLS-DA approach clearly offers great potential for plant metabonomic studies with multiple samples and sample groups. Drying processes led to profound alterations to both the primary and secondary metabolisms of SMB including proline biosynthesis, photosynthesis and carbohydrate metabolisms, protein biosynthesis and shikimate-mediated polyphenol and diterpenoid biosyntheses. Air-drying promoted the biosynthesis of the abundant polyphenolic acids and tanshinones, whereas sun-drying enhanced tanshinone biosynthesis but inhibited polyphenolic acid biosynthesis. Although the effects of osmotic stresses on plant secondary metabolisms may vary significantly for different species, our findings may offer some potentially important metabolic information for the development of drought-tolerant plants, especially crops. These results are also of important values for understanding the processing effects of phytomedicines.

Abbreviations: COSY, $^1H-^1H$ correlated spectroscopy; TOCSY, $^1H-^1H$ total correlation spectroscopy; HSQC, heteronuclear single-quantum coherence; HMBC, heteronuclear multiple-bond correlation; NMR, nuclear magnetic resonance; PCA, principal component analysis; OPLS-DA, orthogonal projection to latent structure discriminant analysis; T_1, spin−lattice relaxation time; FID, Free Induction Decay; FT, Fourier Transformation.

Acknowledgment. We acknowledge the Ministry of Agriculture of the People's Republic of China (2009ZX08012-023B), National Natural Science Foundation of China (20825520) and Chinese Academy of Sciences for financial supports. We thank Prof. Yulan Wang for critical reading of the manuscript and Dr. Hang Zhu of Wuhan Institute of Physics and Mathematics for modifying MATLAB scripts used for color-coded OPLS-DA coefficient plots, which were initially downloaded from the website, http://www.mathworks.com/.

Supporting Information Available: Root samples of *Salvia miltiorrhiza* Bunge (SMB) used in this study. HPLC-MS data for some SMB metabolites. LC-UV chromatograms for SMB extracts; LC-MS chromatograms in the positive and negative MS modes for SMB extracts; OPLS-DA scores and coefficient-coded loadings plots derived from LC-DAD data for SMB extracts; PCA scores plots in the negative and positive MS modes for SMB extracts; OPLS-DA scores and coefficient-coded loadings plots in the negative and positive MS modes for SMB extracts; LC-UV chromatograms for extracts from freeze-dried (FD), sun-dried (SD) and air-dried (AD) SMB roots; LC-MS chromatograms detected in the positive and negative MS modes for extracts from freeze-dried (FD), sun-dried (SD) and air-dried (AD) SMB roots; OPLS-DA scores and coefficient-coded loadings plots derived from LC-DAD data for SMB extracts obtained from freeze-dried (FD), sun-dried (SD) and air-dried (AD) SMB roots; PCA scores plots in the negative and positive MS modes for SMB extracts obtained from freeze-dried (FD), sun-dried (SD) and air-dried (AD) SMB roots; OPLS-DA scores and coefficient-coded loadings plots in the negative and positive MS modes for SMB extracts obtained from freeze-dried (FD), sun-dried (SD) and air-dried (AD) SMB roots. This material is available free of charge via the Internet at http://pubs.acs.org.

References

(1) Bogeat-Triboulot, M. B.; Brosche, M.; Renaut, J.; Jouve, L.; Le Thiec, D.; Fayyaz, P.; Vinocur, B.; Witters, E.; Laukens, K.; Teichmann, T.; Altman, A.; Hausman, J. F.; Polle, A.; Kangasjarvi, J.; Dreyer, E. Gradual soil water depletion results in reversible changes of gene expression, protein profiles, ecophysiology, and growth performance in *Populus euphratica*, a poplar growing in arid regions. *Plant Physiol.* **2007**, *143*, 876–892.

(2) Xiong, L. M.; Schumaker, K. S.; Zhu, J. K. Cell signaling during cold, drought, and salt stress. *Plant Cell* **2002**, *14*, S165–S183.

(3) Tolleter, D.; Jaquinod, M.; Mangavel, C.; Passirani, C.; Saulnier, P.; Manon, S.; Teyssier, E.; Payet, N.; Avelange-Macherel, M. H.; Macherel, D. Structure and function of a mitochondrial late embryogenesis abundant protein are revealed by desiccation. *Plant Cell* **2007**, *19*, 1580–1589.

(4) Valliyodan, B.; Nguyen, H. T. Understanding regulatory networks and engineering for enhanced drought tolerance in plants. *Curr. Opin. Plant Biol.* **2006**, *9*, 189–195.

(5) Charlton, A. J.; Donarski, J. A.; Harrison, M.; Jones, S. A.; Godward, J.; Oehlschlager, S.; Arques, J. L.; Ambrose, M.; Chinoy, C.; Mullineaux, P. M.; Domoney, C. Responses of the pea (*Pisum sativum* L.) leaf metabolome to drought stress assessed by nuclear magnetic resonance spectroscopy. *Metabolomics* **2008**, *4*, 312–327.

(6) Nicholson, J. K.; Lindon, J. C.; Holmes, E. 'Metabonomics': understanding the metabolic responses of living systems to pathophysiological stimuli *via* multivariate statistical analysis of biological NMR spectroscopic data. *Xenobiotica* **1999**, *29*, 1181–1189.

(7) Tang, H. R.; Wang, Y. L. Metabonomics: a revolution in progress. *Prog. Biochem. Biophys.* **2006**, *33*, 401–417.

(8) Yap, I. K. S.; Clayton, T. A.; Tang, H.; Everett, J. R.; Hanton, G.; Provost, J. P.; Le Net, J. L.; Charuel, C.; Lindon, J. C.; Nicholson, J. K. An integrated metabonomic approach to describe temporal metabolic disregulation induced in the rat by the model hepatotoxin allyl formate. *J. Proteome Res.* **2006**, *5*, 2675–2684.

(9) Wang, Y. L.; Holmes, E.; Tang, H. R.; Lindon, J. C.; Sprenger, N.; Turini, M. E.; Bergonzelli, G.; Fay, L. B.; Kochhar, S.; Nicholson, J. K. Experimental metabonomic model of dietary variation and stress interactions. *J. Proteome Res.* **2006**, *5*, 1535–1542.

(10) Fiehn, O.; Kopka, J.; Dormann, P.; Altmann, T.; Trethewey, R. N.; Willmitzer, L. Metabolite profiling for plant functional genomics. *Nat. Biotechnol.* **2000**, *18*, 1157–1161.

(11) Raamsdonk, L. M.; Teusink, B.; Broadhurst, D.; Zhang, N. S.; Hayes, A.; Walsh, M. C.; Berden, J. A.; Brindle, K. M.; Kell, D. B.; Rowland, J. J.; Westerhoff, H. V.; van Dam, K.; Oliver, S. G. A functional genomics strategy that uses metabolome data to reveal the phenotype of silent mutations. *Nat. Biotechnol.* **2001**, *19*, 45–50.

(12) Brindle, J. T.; Antti, H.; Holmes, E.; Tranter, G.; Nicholson, J. K.; Bethell, H. W. L.; Clarke, S.; Schofield, P. M.; McKilligin, E.; Mosedale, D. E.; Grainger, D. J. Rapid and noninvasive diagnosis of the presence and severity of coronary heart disease using ^{1}H NMR-based metabonomics. *Nat. Med.* **2002**, *8*, 1439–1444.

(13) Yang, Y. X.; Li, C. L.; Nie, X.; Feng, X. S.; Chen, W. X.; Yue, Y.; Tang, H. R.; Deng, F. Metabonomic studies of human hepatocellular carcinoma using high-resolution magic-angle spinning ^{1}H NMR spectroscopy in conjunction with multivariate data analysis. *J. Proteome Res.* **2007**, *6*, 2605–2614.

(14) Wang, Y. L.; Utzinger, J.; Saric, J.; Li, J. V.; Burckhardt, J.; Dirnhofer, S.; Nicholson, J. K.; Singer, B. H.; Brun, R.; Holmes, E. Global metabolic responses of mice to *Trypanosoma brucei brucei* infection. *Proc. Natl. Acad. Sci. U.S.A.* **2008**, *105*, 6127–6132.

(15) Bundy, J. G.; Lenz, E. M.; Bailey, N. J.; Gavaghan, C. L.; Svendsen, C.; Spurgeon, D.; Hankard, P. K.; Osborn, D.; Weeks, J. A.; Trauger, S. A.; Speir, P.; Sanders, I.; Lindon, J. C.; Nicholson, J. K.; Tang, H. R. Metabonomic assessment of toxicity of 4-fluoroaniline, 3,5-difluoroaniline and 2-fluoro-4-methylaniline to the earthworm *Eisenia veneta* (Rosa): Identification of new endogenous biomarkers. *Environ. Toxicol. Chem.* **2002**, *21*, 1966–1972.

(16) Ding, L. N.; Hao, F. H.; Shi, Z. M.; Wang, Y. L.; Zhang, H. X.; Tang, H. R.; Dai, J. Y. Systems biological responses to chronic perfluorododecanoic acid exposure by integrated metabonomic and transcriptomic studies. *J. Proteome Res.* **2009**, *8*, 2882–2891.

(17) Charlton, A. J.; Farrington, W. H. H.; Brereton, P. Application of ^{1}H NMR and multivariate statistics for screening complex mixtures: Quality control and authenticity of instant coffee. *J. Agric. Food Chem.* **2002**, *50*, 3098–3103.

(18) Duarte, I.; Barros, A.; Belton, P. S.; Righelato, R.; Spraul, M.; Humpfer, E.; Gil, A. M. High-resolution nuclear magnetic resonance spectroscopy and multivariate analysis for the characterization of beer. *J. Agric. Food Chem.* **2002**, *50*, 2475–2481.

(19) Le Gall, G.; Colquhoun, I. J.; Defernez, M. Metabolite profiling using ^{1}H NMR spectroscopy for quality assessment of green tea, *Camellia sinensis* (L.). *J. Agric. Food Chem.* **2004**, *52*, 692–700.

(20) Bailey, N. J. C.; Wang, Y. L.; Sampson, J.; Davis, W.; Whitcombe, I.; Hylands, P. J.; Croft, S. L.; Holmes, E. Prediction of antiplasmodial activity of *Artemisia annua* extracts: application of ^{1}H NMR spectroscopy and chemometrics. *J. Pharm. Biomed. Anal.* **2004**, *35*, 117–126.

(21) Wang, Y. L.; Tang, H. R.; Nicholson, J. K.; Hylands, P. J.; Sampson, J.; Whitcombe, I.; Stewart, C. G.; Caiger, S.; Oru, I.; Holmes, E. Metabolomic strategy for the classification and quality control of phytomedicine: A case study of chamomile flower (*Matricaria recutita* L.). *Planta Med.* **2004**, *70*, 250–255.

(22) Choi, Y. H.; Sertic, S.; Kim, H. K.; Wilson, E. G.; Michopoulos, F.; Lefeber, A. W. M.; Erkelens, C.; Kricun, S. D. P.; Verpoorte, R. Classification of Ilex species based on metabolomic fingerprinting using nuclear magnetic resonance and multivariate data analysis. *J. Agric. Food Chem.* **2005**, *53*, 1237–1245.

(23) Rasmussen, B.; Cloarec, O.; Tang, H. R.; Staerk, D.; Jaroszewski, J. W. Multivariate analysis of integrated and full-resolution ^{1}H NMR spectral data from complex pharmaceutical preparations: St. John's wort. *Planta Med.* **2006**, *72*, 556–563.

(24) Sieveking, D. P.; Woo, K. S.; Fung, K. P.; Lundman, P.; Nakhla, S.; Celermajer, D. S. Chinese herbs danshen and gegen modulate key early atherogenic events *in vitro*. *Int. J. Cardiol* **2005**, *105*, 40–45.

(25) Sugiyama, A.; Zhu, B. M.; Takahara, A.; Satoh, Y.; Hashimoto, K. Cardiac effects of *Salvia miltiorrhiza/Dalbergia odorifera* mixture, an intravenously applicable Chinese medicine widely used for patients with ischemic heart disease in China. *Circ. J.* **2002**, *66*, 182–184.

(26) Wasser, S.; Ho, J. M. S.; Ang, H. K.; Tan, C. E. L. *Salvia miltiorrhiza* reduces experimentally-induced hepatic fibrosis in rats. *J. Hepatol.* **1998**, *29*, 760–771.

(27) Chen, C.; Tang, H. R.; Sutcliffe, L. H.; Belton, P. S. Green tea polyphenols react with 1,1-diphenyl-2-picrylhydrazyl free radicals

in the bilayer of liposomes: Direct evidence from electron spin resonance studies. *J. Agric. Food Chem.* **2000**, *48*, 5710–5714.
(28) Zhang, K. Q.; Bao, Y. D.; Wu, P.; Rosen, R. T.; Ho, C. T. Antioxidative components of tanshen (*Salvia miltiorrhiza* Bung). *J. Agric. Food Chem.* **1990**, *38*, 1194–1197.
(29) Onitsuka, M.; Fujiu, M.; Shinma, N.; Maruyama, H. B. New platelet aggregation inhibitors from Tan-Shen; Radix of *Salvia miltiorrhiza* Bunge. *Chem. Pharm. Bull.* **1983**, *31*, 1670–1675.
(30) Baillie, A. C.; Thomson, R. H. Naturally occurring quinones. Part XI. tanshinones. *J. Chem. Soc. C* **1968**, *4*, 8–52.
(31) Xiao, C. N.; Dai, H.; Liu, H. B.; Wang, Y. L.; Tang, H. R. Revealing the metabonomic variation of rosemary extracts using ^{1}H NMR spectroscopy and multivariate data analysis. *J. Agric. Food Chem.* **2008**, *56*, 10142–10153.
(32) Drew, S. W.; Demain, A. L. Effect of primary metabolites on secondary metabolism. *Annu. Rev. Microbiol.* **1977**, *31*, 343–356.
(33) Lim, Y. Y.; Murtijaya, J. Antioxidant properties of *Phyllanthus amarus* extracts as affected by different drying methods. *LWT–Food Sci. Technol.* **2007**, *40*, 1664–1669.
(34) Kade, I. J.; Ibukun, E. O.; Nogueira, C. W.; da Rocha, J. B. T. Sun-drying diminishes the antioxidative potentials of leaves of *Eugenia uniflora* against formation of thiobarbituric acid reactive substances induced in homogenates of rat brain and liver. *Exp. Toxicol. Pathol.* **2008**, *60*, 365–371.
(35) Chan, E. W. C.; Lim, Y. Y.; Wong, S. K.; Lim, K. K.; Tan, S. P.; Lianto, F. S.; Yong, M. Y. Effects of different drying methods on the antioxidant properties of leaves and tea of ginger species. *Food Chem.* **2009**, *113*, 166–172.
(36) Dean, J. R.; Liu, B.; Price, R. Extraction of tanshinone IIA from *Salvia miltiorrhiza* Bunge using supercritical fluid extraction and a new extraction technique, phytosol solvent extraction. *J. Chromatogr., A* **1998**, *799*, 343–348.
(37) Pan, X. J.; Niu, G. G.; Liu, H. Z. Comparison of microwave-assisted extraction and conventional extraction techniques for the extraction of tanshinones from *Salvia miltiorrhiza* Bunge. *Biochem. Eng. J.* **2002**, *12*, 71–77.
(38) Trygg, J.; Wold, S. Orthogonal projections to latent structures (O-PLS). *J. Chemometr.* **2002**, *16*, 119–128.
(39) Cloarec, O.; Dumas, M. E.; Trygg, J.; Craig, A.; Barton, R. H.; Lindon, J. C.; Nicholson, J. K.; Holmes, E. Evaluation of the orthogonal projection on latent structure model limitations caused by chemical shift variability and improved visualization of biomarker changes in ^{1}H NMR spectroscopic metabonomic studies. *Anal. Chem.* **2005**, *77*, 517–526.
(40) Fan, W. M. T. Metabolite profiling by one and two dimensional NMR analysis of complex mixtures. *Prog. Nucl. Magn. Reson. Spectrosc.* **1996**, *28*, 161–219.
(41) Liu, A. H.; Lin, Y. H.; Yang, M.; Guo, H.; Guan, S. H.; Sun, J. H.; Guo, D. A. Development of the fingerprints for the quality of the roots of *Salvia miltiorrhiza* and its related preparations by HPLC-DAD and LC-MS^n. *J. Chromatogr., B* **2007**, *846*, 32–41.
(42) Yang, M.; Liu, A. H.; Guan, S. H.; Sun, J. H.; Xu, M.; Guo, D. Characterization of tanshinones in the roots of *Salvia miltiorrhiza* (Dan-shen) by high-performance liquid chromatography with electrospray ionization tandem mass spectrometry. *Rapid Commun. Mass Spectrom.* **2006**, *20*, 1266–1280.
(43) Pelleschi, S.; Rocher, J. P.; Prioul, J. L. Effect of water restriction on carbohydrate metabolism and photosynthesis in mature maize leaves. *Plant Cell Environ.* **1997**, *20*, 493–503.
(44) Hare, P. D.; Cress, W. A. Metabolic implications of stress-induced proline accumulation in plants. *Plant Growth Regul.* **1997**, *21*, 79–102.
(45) Smirnoff, N.; Cumbes, Q. J. Hydroxyl radical scavenging activity of compatible solutes. *Phytochemistry* **1989**, *28*, 1057–1060.
(46) Rhodes, D.; Handa, S.; Bressan, R. A. Metabolic changes associated with adaptation of plant cells to water stress. *Plant Physiol.* **1986**, *82*, 890–903.
(47) Hu, C. A. A.; Delauney, A. J.; Verma, D. P. S. A bifunctional enzyme (Δ^1-pyrroline-5-carboxylate synthetase) catalyzes the first two steps in proline biosynthesis in plants. *Proc. Natl. Acad. Sci. U.S.A.* **1992**, *89*, 9354–9358.
(48) Delauney, A. J.; Verma, D. P. S. Proline biosynthesis and osmoregulation in plants. *Plant J.* **1993**, *4*, 215–223.
(49) Yoshiba, Y.; Kiyosue, T.; Katagiri, T.; Ueda, H.; Mizoguchi, T.; Yamaguchishinozaki, K.; Wada, K.; Harada, Y.; Shinozaki, K. Correlation between the induction of a gene for Δ^1-pyrroline-5-carboxylate synthetase and the accumulation of proline in *Arabidopsis thaliana* under osmotic stress. *Plant J.* **1995**, *7*, 751–760.
(50) Kiyosue, T.; Yoshiba, Y.; YamaguchiShinozaki, K.; Shinozaki, K. A nuclear gene encoding mitochondrial proline dehydrogenase, an enzyme involved in proline metabolism, is upregulated by proline but downregulated by dehydration in *Arabidopsis*. *Plant Cell* **1996**, *8*, 1323–1335.
(51) Quick, P.; Siegl, G.; Neuhaus, E.; Feil, R.; Stitt, M. Short-term water stress leads to a stimulation of sucrose synthesis by activating sucrose-phosphate synthase. *Planta* **1989**, *177*, 535–546.
(52) Gonzalez, E. M.; Gordon, A. J.; James, C. L.; Arreseigor, C. The role of sucrose synthase in the response of soybean nodules to drought. *J. Exp. Bot.* **1995**, *46*, 1515–1523.
(53) Ramos, M. L. G.; Gordon, A. J.; Minchin, F. R.; Sprent, J. I.; Parsons, R. Effect of water stress on nodule physiology and biochemistry of a drought tolerant cultivar of common bean (*Phaseolus vulgaris* L.). *Ann. Bot.* **1999**, *83*, 57–63.
(54) Ranieri, A.; Bernardi, R.; Lanese, P.; Soldatini, G. F. Changes in free amino-acid content and protein pattern of maize seedlings under water stress. *Environ. Exp. Bot.* **1989**, *29*, 351–357.
(55) Taji, T.; Ohsumi, C.; Iuchi, S.; Seki, M.; Kasuga, M.; Kobayashi, M.; Yamaguchi-Shinozaki, K.; Shinozaki, K. Important roles of drought- and cold-inducible genes for galactinol synthase in stress tolerance in *Arabidopsis thaliana*. *Plant J.* **2002**, *29*, 417–426.
(56) Amiard, V.; Morvan-Bertrand, A.; Billard, J. P.; Huault, C.; Keller, F.; Prud'homme, M. P. Fructans, but not the sucrosyl-galactosides, raffinose and loliose, are affected by drought stress in perennial ryegrass. *Plant Physiol.* **2003**, *132*, 2218–2229.
(57) Avelange-Macherel, M. H.; Ly-Vu, B.; Delaunay, J.; Richomme, P.; Leprince, O. NMR metabolite profiling analysis reveals changes in phospholipid metabolism associated with the re-establishment of desiccation tolerance upon osmotic stress in germinated radicles of cucumber. *Plant Cell Environ.* **2006**, *29*, 471–482.

PR900995M